Arbitrary Energy-Preserving Control of Optical Pulse Trains and Frequency Combs through Generalized Talbot Effects

Luis Romero Cortés, Reza Maram, Hugues Guillet de Chatellus, and José Azaña*

Trains of optical pulses and optical-frequency combs are periodic waveforms with deep implications for a wide range of scientific disciplines and technological applications. Recently, phase-only signal-processing techniques based upon the theory of Talbot self-imaging have been demonstrated as simple and practical means for user-defined periodicity control of optical pulse trains and combs. The resulting schemes implement a desired repetition period control without introducing any noise or distortion, while ideally preserving the entire energy content of the signal. Here, recent developments on phase-only signal-processing schemes for periodicity control based on temporal and spectral self-imaging are reviewed. As a central contribution, a comprehensive theory of generalized Talbot self-imaging, so called phase-controlled Talbot effect, is presented, comprising all the different approaches proposed to date. In particular, a closed unified mathematical framework for the design of the spectral and temporal phase manipulations that enable full arbitrary control of the period of repetitive signals is developed. The reported numerical studies fully validate the presented theoretical framework and shed light on crucial aspects of the proposed methods, consistently with previously reported experimental results. Important considerations concerning the practical, real-world implementation of the described schemes, according to the needed specifications for different applications, are also discussed.

1. Introduction

Since the first demonstrations of optical phase-locking and the first mode-locked laser developments,[1] the capability to generate precisely timed periodic trains of optical pulses has pushed forward many fields of science and technology. Extensive effort has been further devoted to the generation and control of optical frequency combs,[2–14] the frequency-domain counterpart of time-periodic coherent optical pulse trains. A frequency comb consists of a set of equally-spaced spectral components (comb lines), with a frequency spacing referred to as the free spectral range (FSR). Periodic optical pulse trains and frequency combs are key elements for a myriad of scientific developments and technological applications of great relevance, including among others, ultrafast optical and microwave signal generation and processing,[15–19] generation of Terahertz pulses,[20] high-resolution spectroscopy,[21–24] high-precision frequency metrology,[25] high-accuracy frequency calibration (e.g., as used in astronomical telescopes),[26–29] high-capacity telecommunication systems,[30–34] and more recently, promising new avenues for quantum computing.[35–38]

A fundamental parameter of these signals is their period of repetition: the pulse period, t_r, of a pulse train, or the FSR, v_r, of a frequency comb. Not only most applications require that this parameter is fixed with precision (e.g., the rate at which information is transmitted in a telecommunication system is strongly related to the period of the clock signal[39]), but distinct applications require fundamentally different orders of magnitude. For instance, typical atomic and molecular spectroscopy applications require combs with FSR values in the MHz regime,[24] while astronomical spectrographic measurements,[28] as well as applications aimed at arbitrary waveform generation

Dr. L. Romero Cortés, Dr. R. Maram, Prof. H. Guillet de Chatellus, Prof. J. Azaña
Institut National de la Recherche Scientifique – Énergie
Matériaux et Télécommunications (INRS–EMT)
Montréal, QC H5A 1K6, Canada
E-mail: romero@emt.inrs.ca

The ORCID identification number(s) for the author(s) of this article can be found under https://doi.org/10.1002/lpor.201900176

Dr. R. Maram
Department of Electrical and Computer Engineering
McGill University
Montréal, QC H3A 0E9, Canada

Prof. H. Guillet de Chatellus
Centre National de la Recherche Scientifique (CNRS)
Université Grenoble Alpes
38000 Grenoble, France

Prof. H. Guillet de Chatellus
Laboratoire Interdisciplinaire de Physique (LIPhy)
Université Grenoble Alpes
38000 Grenoble, France

and processing,[16,19] are performed with combs in the GHz regime. Techniques for manipulating the period of repetitive signals are thus key for such applications. Optical pulse trains (and their frequency comb spectra) are commonly generated using mode-locked lasers. These typically offer a limited flexibility to design –and subsequently control– the repetition rate of the generated optical signal. For instance, integrated micro-cavity lasers are suitable for generation of periodic optical waveforms with repetition rates in the GHz regime, while longer cavities, such as those used in fiber-based mode-locked lasers, provide access to repetition rates in the MHz regime.[40] In order to control the periodicity of the signals generated by these systems, one must either modify the physical parameters of the laser cavity,for example, its length (impractical or simply not possible in most situations), or resort to techniques such as harmonic mode-locking, which typically results in a highly distorted output signal with degraded signal-to-noise ratio.[41,42] This calls for the need of periodicity control through signal processing of the generated repetitive waveforms outside the laser cavity.

Conventional periodicity control solutions based on signal processing operations rely on wave transformations that directly affect the energy content of the signal (e.g., spectral amplitude filtering and temporal amplitude modulation); these methods present critical shortcomings, not least of which is their inherent energy inefficiency (briefly discussed in Section 2). Signal processing solutions based on phase-only manipulations are particularly attractive,[43] as they recycle the energy carried by the input signal into an output signal that satisfies the required specifications.[44–50]

This review focuses on energy-preserving periodicity control methods based on phase-only signal processing operations based upon the theory of the Talbot effect.[51–56] Temporal Talbot effect has been used to reduce the period of a temporal pulse train, dividing it by an integer factor,[57,58] through the use of an SPF process, for example, via dispersive propagation[59] (see **Figure 1**(a.1)). Its frequency domain counterpart, spectral Talbot effect, has been used to reduce the FSR of a frequency comb, dividing it by an integer factor,[60–62] through the use of a temporal phase modulation (TPM) process, for example, via electro-optical interaction[59] (see Figure 1(a.2)). A distinctive feature of temporal and spectral Talbot effects is that they enable manipulation of the repetition rate of an incoming pulse train or the FSR of its corresponding frequency comb spectrum without altering the individual temporal pulse characteristics (i.e., the pulse's complex temporal envelope, including shape and duration) and the spectral envelope of the corresponding frequency comb. Moreover, techniques based on such methodology have been proposed to manipulate the repetition period of pulse trains and frequency combs at will, not limited to integer division.[58,60–68] As illustrated in Figure 1b, these methods involve specific combinations of SPF and TPM operations corresponding to concatenated individual realizations of temporal and spectral Talbot effects. However, all such methods reported to date are incomplete in that they do not provide a full transformation of the signal's repetition period in both the time and frequency domains. As such, the periods of the obtained pulse train and its corresponding frequency comb representation are generally unrelated after application of the method (see Figure 1b). This work provides a closed mathematical description
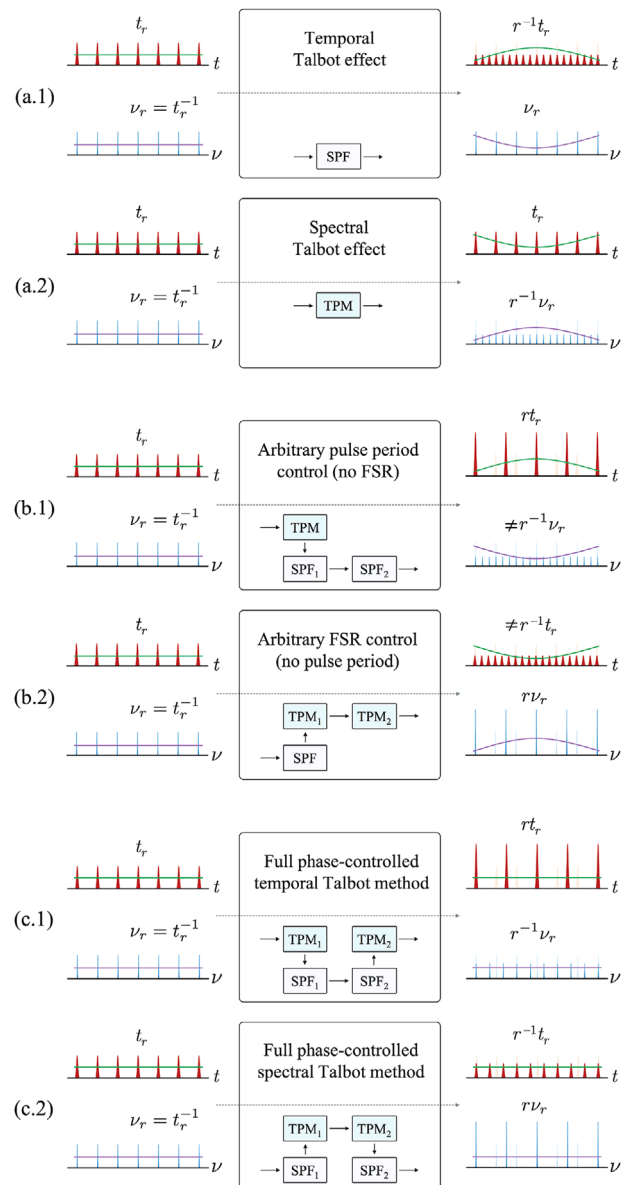

Figure 1. Schemes for repetition period control through phase transformations (SPF: spectral phase filtering; TPM: temporal phase modulation) based on the theory of the Talbot effect. a) Fractional temporal (1) and spectral (2) Talbot effects; the repetition period of a pulse train or frequency comb is divided by an integer factor r; the signal in the dual domain is not modified and residual phase variations remain in both domains. b) Combinations of Talbot phase transformations resulting in an arbitrary control of the pulse period (1) or the FSR (2) of a repetitive signal; the period multiplication factor, r, can take arbitrary (rational) values; the signal representations in both the time and frequency domains have unrelated repetition periods and residual phase variations remain uncompensated. c) Proposed generalization of the repetition period control methods based on dual Talbot effects, i.e., phase-controlled temporal (1) and spectral (2) Talbot methods – the focus of this work, and developed in Section 4; the period multiplication factor, r, can take arbitrary (rational) values; the signal representations in both time and frequency domains have related repetition periods (the phase transformations are completed) and all residual phase variations are compensated.

of Talbot-based arbitrary periodicity control methods, here referred to as "phase-controlled Talbot effect", and formulates the conditions for completing the desired period transformations in both the temporal and spectral domains of the signal of interest. As illustrated in Figure 1c, the theory reported here exploits the recently formalized mathematical symmetry between temporal and spectral realizations of the Talbot effect, so-called "time/frequency duality of self-imaging".[69] Two alternative, equivalent schemes are defined to achieve multiplication or division of the temporal pulse repetition period –and the related frequency spacing manipulation of the corresponding frequency comb spectrum– by any desired integer or fractional factor (see Figure 1c). Closed expressions are derived for calculating the required temporal and spectral phase transformations for arbitrarily tailoring the period of any given repetitive temporal and/or spectral signal of interest.

The paper is structured as follows: Section 2 provides the basic definitions of the relevant parameters of periodic waveforms in their temporal and spectral representations, and briefly describes the most conventional signal processing methods for periodicity control of such waveforms and their drawbacks. Section 3 presents an overview of the fundamental theory of temporal and spectral Talbot effect, upon which the signal processing methods studied and reviewed in this paper are based. Section 4 describes the methodology used in Talbot-based periodicity control signal processing techniques, providing the closed mathematical formulation of generalized phase-controlled Talbot effect (validated through numerical simulation), and including important considerations concerning practical implementations. Section 5 reviews recent experimental work based on the described signal processing methodology. Section 6 provides additional discussions and concludes the paper.

2. Control of the Periodicity of Repetitive Signals

2.1. Fourier Relations for Periodic Signals

A periodic train of optical pulses, $\psi(t)$, and its optical frequency comb counterpart, $\Psi(\nu)$, are related by a Fourier transform.[70] **Figure 2** and Equations (1a) and (1b), illustrate this relationship.

$$\psi(t) = \sum_{n=-\infty}^{\infty} \gamma(t - nt_r) \tag{1a}$$

$$\Psi(\nu) = \sum_{k=-\infty}^{\infty} c_k \delta(\nu - k\nu_r) \tag{1b}$$

where the variables t and ν stand for time and frequency, respectively. These two equations form a Fourier transform pair,
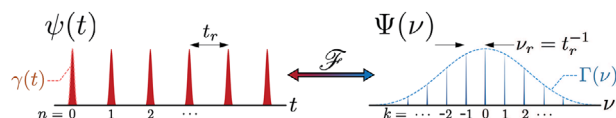

Figure 2. Relationship between a coherent train of optical pulses with period t_r, and its spectral counterpart, a frequency comb with FSR $\nu_r = t_r^{-1}$. The symbol $\mathscr{F}$ denotes the Fourier transform.

so that $\Psi(\nu) = \mathscr{F}\{\psi(t)\}$, where the symbol $\mathscr{F}$ denotes the Fourier transform, $\gamma(t)$ is the temporal complex envelope of an individual pulse, t_r is the repetition period of the train, $\delta(\nu)$ is the unitary Dirac delta function evaluated in the frequency domain, and $\nu_r = t_r^{-1}$ is the FSR. In this situation, the comb FSR dictates the rate at which the pulse train completes a cycle in the time domain, that is, its repetition rate. The coefficient $c_k = \nu_r \Gamma(k\nu_r)$ represents the complex weight of each comb line, where $\Gamma(\nu) = \mathscr{F}\{\gamma(t)\}$ is the complex spectral envelope of the comb. Note that this description only deals with the complex envelope of the involved signals (often referred to as the equivalent base-band representation), and the underlying central frequency, or carrier, is omitted for simplicity. The formal definition of other important parameters, such as the temporal and spectral peak powers and noise content of the signal,[71] has also been omitted for simplicity, as the following mathematical analysis focuses on techniques to manipulate the temporal and spectral periods (t_r and ν_r, respectively).

2.2. Conventional Signal Processing Methods for Periodicity Control

Conventional, well-established approaches for off-cavity periodicity control of arbitrary pulse trains and frequency combs through signal processing include spectral amplitude filtering and temporal pulse picking (or time gating), sketched in **Figure 3**. A spectral amplitude filter is a straight-forward way of directly multiplying the FSR of a frequency comb, simply by eliminating $r - 1$ out of each r consecutive comb lines. This effectively produces an r-fold increase of the FSR, and an associated r-fold reduction of the pulse period of the train.[26,27,72–74] The dual operation is also possible, in the form of pulse picking,[75] where a temporal
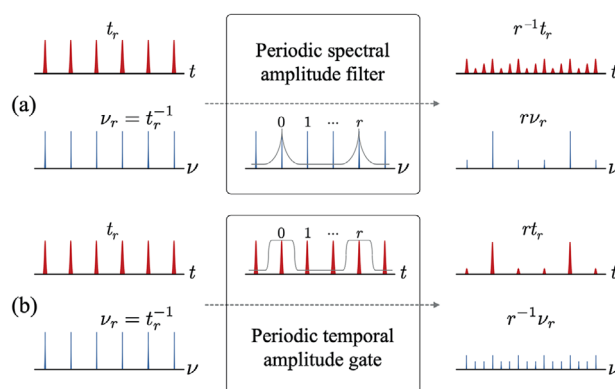

Figure 3. Conventional periodicity control methods for trains of optical pulses and optical frequency combs. a) Spectral amplitude filtering and b) pulse picking by temporal amplitude gating. By construction, these methods only allow periodicity manipulation in integer values of the parameter r. As an example, a period multiplication factor $r = 3$ is shown. Both methods involve the deliberate discarding of a fraction $1 - r^{-1}$ of the original signal energy, resulting in an energy loss that increases with the factor r. Amplification may then become necessary for further processing and/or detection of the signals of interest, thus incurring the associated degradation of the signal-to-noise ratio, unavoidable in classical active processes. Additionally, the imperfect suppression of comb lines (temporal pulses) results in undesired amplitude fluctuations of the output pulse train (frequency comb), thus degrading the quality of the obtained signal.

**ADVANCED
SCIENCE NEWS**

www.advancedsciencenews.com

LASER
& PHOTONICS
REVIEWS

www.lpr-journal.org

amplitude gate selects one pulse out of each r consecutive pulses and throws away the remaining $r - 1$. The repetition period is then directly increased by r, and the associated FSR of the corresponding comb spectrum is reduced by the same factor. The main drawback of these approaches is their low energy efficiency, as they rely on directly discarding signal energy. Additionally, these methods suffer from practical implementation shortcomings. The amplitude filtering method needs high-finesse filters, with tight design and operational requirements (e.g., precise spectral alignment between the filter and the comb), in order to achieve signals with high quality (Figure 3a).[76] Similarly, the imperfect suppression of undesired pulses in pulse picking techniques results in spectral line-to-line amplitude fluctuations of the obtained comb (Figure 3b). The relatively low extinction ratio of current electro-optic intensity modulators often forces to use optical gates based on nonlinear effects (incurring in even higher energy inefficiency), or optical switches based on semiconductor optical amplifiers and acousto-optic modulators (with typically low operation speeds).[77–80] Moreover, a precise timing between the pulse train and the pulse picking gate becomes a critical factor for a correct pulse suppression. Approaches aimed at mitigating the problem of energy loss in pulse picking methods, such as coherent addition of pulses in optical cavities, have also been demonstrated; however these require stringent operation conditions, difficult to achieve and maintain.[81] Last, but not the least, the very nature of these techniques forces the factor r to be necessary integer. This is due to the fact that one can only suppress an integer number of pulses (or frequency lines) through an amplitude gate (or filter). Fractional period multiplication/division could be achieved through combinations of amplitude filtering and pulse picking techniques, suffering from the critical aforementioned drawbacks associated with both methodologies. Versatile methods to control the pulse period of optical trains and the FSR of frequency combs with high energy efficiency and low signal degradation based on passive, linear processes are highly desired.

In order to avoid discarding energy of the signal of interest, a period control method must rely exclusively on manipulations of the phase distributions of the signal in the time and/or frequency domains.[43] This way, the desired output signal is constructed from the recycled energy of the input signal, preventing any loss of energy in the process, except for practical insertion losses. Additionally, such solutions offer an increased tolerance to practical implementation errors, greatly relaxing the design requirements of methods involving direct amplitude manipulations. Considering all these key advantages, several techniques for periodicity control through phase manipulations have been proposed.

In particular, an important set of these techniques is based on the theory of Talbot self-imaging.[58,60–67] Such methods have been developed to achieve multiplication and/or division of the repetition period of pulse trains by arbitrary (integer or fractional) factors,[58,63–65] as well as arbitrary control of the FSR of frequency combs.[60–62,66–68] Furthermore, due to the inherent phase-only nature of these approaches, the entire energy of the processed signal is ideally preserved; as a result, these methods are able to reduce the impact of noise and signal aperiodicities (such as timing jitter and pulse-to-pulse intensity fluctuations) under certain operation conditions.[63,65,67,82] The following section provides a brief overview of the temporal and spectral Talbot self-imaging effects.

3. Overview of Temporal and Spectral Talbot Effects

Talbot effects, also known as self-imaging effects, have received a great deal of attention through the last decades.[53,56] These phenomena manifest when a wave exhibiting periodicity on one of its representation domains (i.e., space, transverse momentum, time or frequency) is affected by a propagator imposing a specific quadratic phase profile across the Fourier-dual of such domain. The mathematical definition of these phase profiles is known as the "Talbot condition."[69] This gives rise to perfect images of the wave (integer self-imaging) or to sub-images where the initial period is divided by a natural number (fractional self-imaging).

Although the effect was initially observed and explained in the context of Fresnel diffraction of spatially periodic waves,[51,52] its description was extended to the time domain[57,58] through the application of the well-known space–time duality.[83,84] Such a duality is a powerful mathematical tool that relates the equations describing the propagation of spatial wavefronts in free space and the propagation of temporal waveforms through dispersive optical media. This theoretical framework has opened the door to a myriad of time- and frequency-domain linear and nonlinear optical signal processing applications inspired by free space optics systems.[85]

More recently, Talbot effect was predicted and observed in the frequency[60–62] and transverse momentum (observed in the form of angular spectrum)[86] domains of optical waves. These latest manifestations can be explained on the basis of the time/frequency duality,[87] or, more generally, Fourier duality, of Talbot self-imaging, that is, a symmetry in the laws governing the effect in observation domains related by a Fourier transform.[69]

Since our main focus is on the control of optical trains and frequency combs, we pay attention to the temporal and spectral manifestations of the effect; however, it is worth mentioning that all the results presented in this work are immediately applicable to the space and transverse momentum domains as well, through direct application of the space–time duality.[83]

3.1. Temporal Talbot Effect

The temporal Talbot effect, represented in **Figure 4**a, is observed when a periodic train of optical pulses, with period t_r, propagates through a transparent medium presenting a certain amount of second-order group-velocity dispersion (GVD).[58] This process can be described as a unitary phase filter, with a spectral transfer function, $\mathscr{H}(\omega)$, given by

$$\mathscr{H}(\omega) = e^{-i\frac{1}{2}\beta_2 z \omega^2} \tag{2}$$

where i is the imaginary unit, β_2 is the second-order dispersion coefficient of the medium (GVD per unit length, measured at the central frequency of the wave), z is the propagation length, and $\omega = 2\pi\nu$.[59] Notice the quadratic phase variation as a function of the Fourier-domain variable, ω, as anticipated above. Equation 4 describes the simplified transfer function of a general transparent propagation medium, were β_2 corresponds to the second-order Taylor coefficient of the medium's spectral phase distribution. The constant and linear phase terms, corresponding to
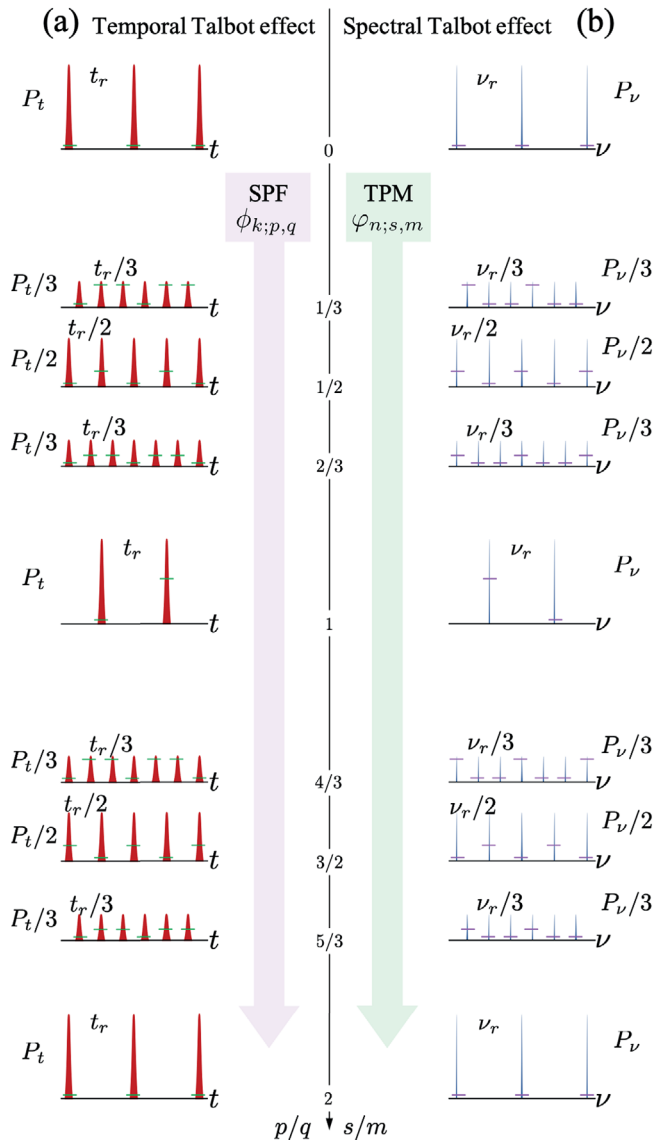
**ADVANCED
SCIENCE NEWS**

www.advancedsciencenews.com

LASER
& PHOTONICS
REVIEWS

www.lpr-journal.org

Figure 4. Representation of the formation of temporal and spectral Talbot images and sub-images. a) Temporal Talbot (sub-)images of a train of pulses generated by spectral phase filtering (SPF); the instantaneous power distribution of the pulses is shown in red, while the acquired temporal phase sequence is shown in green. b) Spectral Talbot (sub-)images of a frequency comb generated by temporal phase modulation (TPM); the power spectral density of the comb is shown in blue, while the acquired spectral phase sequence is shown in purple. The output Talbot (sub-)images are obtained for specific values of quadratic SPF or TPM (determined by the fractions p/q and s/m in Equations (4) and (6)).

a mere average group delay of the resulting temporal sequence, are not considered in this analysis. Additionally, high-order phase terms are assumed to be negligible.

The main assumption here is that all pulses of the sequence are identical, regardless of the particular amplitude and phase profiles of their complex envelope, $\gamma(t)$. It should be noted however that works on Talbot effect of aperiodic waves have been conducted, leading to practical applications such as temporal clock recovery techniques[88,89] and restoration of faulty spatial

images.[90–92] In what concerns the basic temporal Talbot effect, no particular restrictions are imposed to the complex amplitude envelope of the individual pulses in the input sequence ($\gamma(t)$ in Equation (1a) can take any value); however, the temporal duration of the individual pulses will limit the amount of observable Talbot sub-images (this will be addressed in more detail in Section 4.3.1). The temporal Talbot condition provides the required amount of GVD, necessary to obtain a specific Talbot (sub-)image.[58]

$$2\pi|\beta_2|z = \frac{p}{q}t_r^2 \tag{3}$$

where p and q are two mutually prime natural numbers. The pulse train obtained at the output of the dispersive medium has a pulse period $q^{-1}t_r$ (see Figure 4a), while the FSR of its comb spectrum remains unaltered. Since the process only involves a spectral phase manipulation, the total input energy is redistributed into a pulse train with a higher repetition rate; as such, the output energy per pulse corresponds to the input energy per pulse divided by q. As mentioned above, this repetition rate multiplication process is produced without altering the temporal features (temporal duration and shape) of the individual pulses in the obtained train.

Owing to the discrete nature of the spectral comb representation of the train, we can write a discrete form of the temporal Talbot condition[69] as follows:

$$\phi_{k;p,q} = \sigma\pi\frac{p}{q}k^2 \tag{4}$$

where σ is the sign of the second-order dispersion coefficient

$$\sigma = \begin{cases} -1 & \forall\,\beta_2 < 0 \\ 0 & \forall\,\beta_2 = 0 \\ 1 & \forall\,\beta_2 > 0 \end{cases} \tag{5}$$

The coefficient $\phi_{k;p,q}$ represents the required amount of spectral phase-shift to be applied to the k-th line of the corresponding frequency comb to satisfy the condition of the Talbot image labeled by p/q; for example, $k = 0, \pm1, \pm2, \ldots$, where $k = 0$ represents the line at the central frequency of the comb. Equation (4) can be easily derived by evaluating the spectral phase transfer function of the dispersive medium in Equation 4 at the discrete frequency locations of the comb representation, that is, $\sphericalangle\mathcal{H}(\omega)|_{\omega=2k\pi\nu_r}$, under the Talbot condition in Equation (3).

A key feature of this effect is that the obtained period-divided pulse train acquires a pulse-to-pulse temporal phase profile. These temporal Talbot phases are deterministic,[54,55] and were recently shown to also satisfy a Talbot condition.[69] Neglecting a constant factor, these phases write as follows:

$$\varphi_{n;s,m} = -\sigma\pi\frac{s}{m}n^2 \tag{6}$$

where s and m are two mutually prime natural numbers, $m = q$, and s and q have opposite parity.[69,93]

The coefficient $\varphi_{n;s,m}$ represents the phase-shift acquired by the n-th pulse of the output sequence ($n = 0, \pm1, \pm2, \ldots$). The values of s depend only on p and q, and are determined by the parity of the product pq. In particular, if $\mathbb{E}$ denotes the set of even

**ADVANCED
SCIENCE NEWS**

www.advancedsciencenews.com
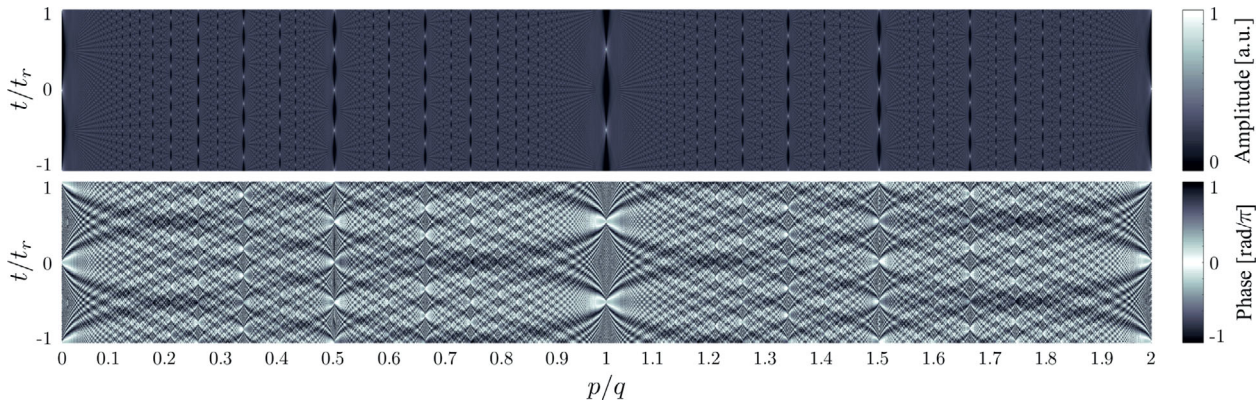
LASER
& PHOTONICS
REVIEWS

www.lpr-journal.org

Figure 5. Normalized amplitude (top) and phase (bottom) Talbot carpets. In order to produce this picture, the ratio p/q takes real values in the fundamental range [0,2] (the Talbot carpet is periodic and repeats outside of this interval ref. [69]). It is important to note that Talbot images form only at rational values of p/q, that is, where p and q are mutually prime natural numbers.

natural numbers and $\mathbb{O}$ denotes the set of odd natural numbers, the parameter s takes the following values

$$s = \begin{cases} p\left(\left[\frac{1}{p}\right]_q\right)^2 & \forall\, pq \in \mathbb{E} \\ 8p\left[\frac{1}{2}\right]_q\left(\left[\frac{1}{2p}\right]_q\right)^2 & \forall\, pq \in \mathbb{O} \end{cases} \tag{7}$$

where $[1/x]_q$ is the modular multiplicative inverse of x modulo q, that is, the (unique) positive integer smaller than q satisfying $x[1/x]_q = 1 \;(\mathrm{mod}\; q)$.[69] A more compact form of this solution for the parameter s was recently found[93]

$$sp = 1 + q\epsilon_q\,(\mathrm{mod}\; 2q) \tag{8}$$

where ϵ_q is the parity of q, that is,

$$\epsilon_q = \begin{cases} 0 & \forall\, q \in \mathbb{E} \\ 1 & \forall\, q \in \mathbb{O} \end{cases} \tag{9}$$

Figure 5 represents the output temporal waveform obtained for each value of the ratio p/q. The result is a periodic structure known as the "Talbot carpet." This picture contains all possible Talbot images and sub-images. Figure 4a shows a more detailed representation of the formation of temporal Talbot images and sub-images for different values of p and q.

As an additional note, it is interesting to remark that, if reduced modulo 2π, the applied spectral phase sequence, $\phi_{k;p,q}$ in Equation (4), is q-periodic when $pq \in \mathbb{E}$, and $2q$-periodic when $pq \in \mathbb{O}$. On the other hand, the induced temporal phase sequence, $\varphi_{n;s,m}$, is always m-periodic because Equations (7) and (8) ensure that $sm \in \mathbb{E}$.[69]

3.2. Spectral Talbot Effect

The expression of the temporal Talbot phases given by Equation (6) satisfies a Talbot condition, that is, its expression is isomorphic to the spectral Talbot phase, given by Equation (4), necessary to produce a temporal Talbot effect. We refer to this

mathematical symmetry as the time/frequency duality (more generally, the Fourier duality) of the Talbot effect.[69] On the basis of this duality, a spectral version of the phenomenon, represented in Figure 4b, can then be observed in the frequency domain. In particular, when the temporal phase-shift, $\varphi_{n;s,m}$, (see Equation (6)) is introduced to the n-th pulse of a train, originally free of pulse-to-pulse phase variations, the FSR of its frequency comb spectrum is divided by the integer factor m.

For a practical implementation on optical pulses, the use of cross-phase-modulation with a continuous parabolic pump pulse train was first proposed,[60] and subsequently demonstrated.[66] An alternative, convenient practical implementation involves the use of an electro-optic temporal phase modulator driven by a periodic step-like modulation function –for example, generated from an electronic arbitrary waveform generator– that follows the exact temporal phase profile prescribed by the theory of Talbot effect.[62]

Similarly to the temporal Talbot effect, the output FSR-divided comb acquires a line-to-line spectral phase profile, $\phi_{k;p,q}$, given by Equation (4) (see Figure 4b), where the value of the parameter p is again determined by Equation (8).

A spectral version of the Talbot carpet can be represented, obtaining a picture similar to the one depicted in Figure 5, with the appropriate variable changes, $p \leftarrow s$, $q \leftarrow m$, $t \leftarrow \nu$ and $t_r \leftarrow \nu_r$. A more detailed representation of the formation of spectral Talbot images and sub-images is shown in Figure 4b.

The periodicity of the Talbot phases in the spectral Talbot effect is now governed by the parity of the product sm. In particular, if reduced modulo 2π, the applied temporal phase sequence, $\varphi_{n;s,m}$, is m-periodic when $sm \in \mathbb{E}$, and $2m$-periodic when $sm \in \mathbb{O}$, while the induced spectral phase sequence, $\phi_{k;p,q}$, is always q-periodic.[69]

3.3. Transformations in the Talbot Carpet

The application of a specific Talbot phase can be interpreted as a displacement from one point in the Talbot carpet to a different one. This visual way of interpreting the effect is particularly useful to picture the transformations involved in the model for
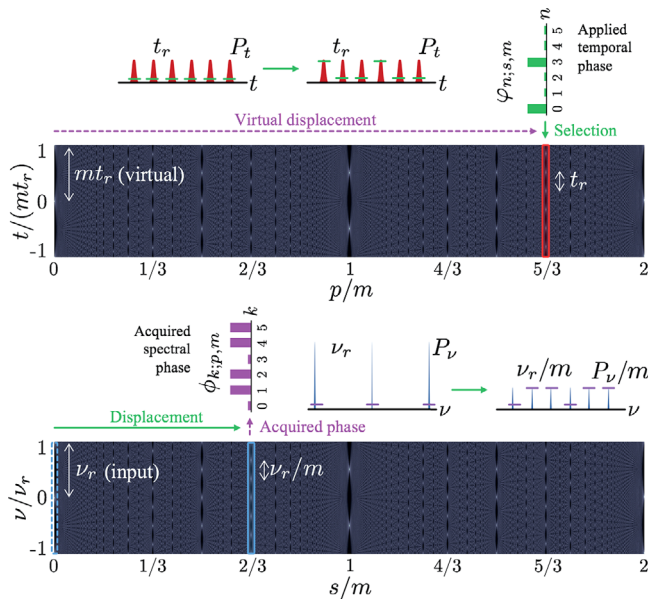
ADVANCED
SCIENCE NEWS

www.advancedsciencenews.com

LASER
& PHOTONICS
REVIEWS

www.lpr-journal.org

Figure 6. Manipulation of Talbot phases described as transformations in the Talbot carpet. The temporal phase $\varphi_{n;s,m}$ applied to a train of pulses with period t_r (top) produces the sub-image s/m of a fractional spectral Talbot effect (bottom). Moreover, the output train behaves as the sub-image p/m of a "virtual" temporal Talbot carpet with input period mt_r (as illustrated in the top figure). Note that, in general, $p \neq s$; in the given example, $s = 2$ and $m = 3$, resulting in $p = 5$.

periodicity control that is at the core of our work reported here, as detailed in the following section.

To illustrate this, let us consider a train of pulses with period t_r, to which we apply a temporal Talbot phase $\varphi_{n;s,m}$ (from Equation (6)), satisfying a spectral Talbot condition for the pair $\{s, m\}$. **Figure 6** shows the effect of such a phase transformation along the spectral and temporal amplitude Talbot carpets. The applied temporal phase divides the input FSR by m (as shown in the bottom plot of Figure 6), and this is equivalent to 'transporting' the plane 0 to the plane s/m in the spectral carpet. The outcome of this TPM is then a spectral Talbot effect. The input pulse period remains unaltered, but the applied temporal phase emulates the effect of dispersive propagation of a virtual pulse train with original period mt_r, to the temporal sub-image p/m (as shown in the top plot of Figure 6). This corresponds to a spectral phase $\phi_{k;p,m}$ (from Equation 4), acquired by the FSR-divided comb. The applied temporal phase has then the effect of selecting a sub-image, p/m, in a virtual temporal carpet where the period of the virtual pulse train at the input (plane 0) is m times the period of the real pulse train under analysis (see Figure 6, top). Equivalently, this corresponds to a displacement on the spectral carpet to a, generally different, sub-image s/m. Note that while the denominator m is the same in both domains, in general, $p \neq s$.[69]

The dual situation, i.e., temporal Talbot effect, would be produced by the SPF of a frequency comb with a Talbot phase sequence $\phi_{k;p,q}$. In such case, the resulting transformations would be the selection of the sub-image s/q in a virtual spectral Talbot carpet with an input FSR q times larger than that of the real comb under analysis, and a displacement on the temporal carpet to the sub-image p/q.

4. Phase-Controlled Talbot Effects

The functional forms of the temporal and spectral Talbot phases (Equations (4) and (6), respectively), and their relationship (Equation (8)), provide the key to achieve an arbitrary control of the repetition period of a pulse train or a frequency comb. For this purpose, one simply must find and apply the right recipe of Talbot phases. In particular, one could select a specific Talbot image or sub-image as the input signal, and then induce a displacement to a different Talbot image or sub-image with the desired period in the same carpet, obtaining the output signal. The transformations required to achieve such arbitrary control of periodicity are detailed in this section.

Two different, though equivalent, methods can be designed to arbitrarily set the repetition period of the train/comb of interest. These two methods differ by the order in which the specific Talbot phases are applied. We name them by "phase-controlled temporal Talbot method" (**Figure 7**a) and "phase-controlled spectral Talbot method" (Figure 7b), respectively.

4.1. Phase-Controlled Temporal Talbot Method

Here, we define a generalized version of the temporal Talbot effect, that is, a method to transform a train of optical pulses with period t_r into a new train with period rt_r, where the multiplication factor of the repetition period, r, can be any irreducible fraction, that is, $r \in \mathbb{Q}$. In general, r is a rational number, such that $r = q_2^{-1} q_1 \forall \{q_1, q_2\} \in \mathbb{N}$ and $\{q_1, q_2\}$ is a co-prime pair. If the transformation is entirely completed, in the frequency domain, this translates into a division of the corresponding frequency comb FSR by the factor r, that is, from $\nu_r = t_r^{-1}$ to $r^{-1}\nu_r$. Different combinations of temporal and spectral Talbot phases could be designed to achieve the same multiplication factor; that is, different values of the parameters p, q, s, and m in Equations (4) and (6). We describe the general solution of the problem and then provide guidelines to achieve particular solutions that minimize the displacement on the temporal Talbot carpet (corresponding to the case of minimum required dispersion in a practical implementation).

4.1.1. General Solution with Perfect Phase Cancellation

The general phase-controlled temporal Talbot method, depicted in Figure 7a, consists of the following four steps:

0. *Input*: The starting point is a pulse train with period t_r, corresponding to a frequency comb with FSR $\nu_r = t_r^{-1}$ (Figure 7(a.0)). The goal is to achieve a train with period rt_r, with $r \in \mathbb{Q}$, that is, $r = q_2^{-1} q_1 \forall \{q_1, q_2\} \in \mathbb{N}$.

1. *TPM₁ (temporal phase modulation 1)*: The input train is temporally phase-modulated with the sequence $\varphi_{n;s_1,q_1}$, corresponding to a spectral Talbot condition s_1/q_1 (see Equation (6)). The resulting frequency comb has an FSR $q_1^{-1}\nu_r$, while the pulse period remains equal to t_r (Figure 7(a.1)).

2. *SPF₁ (spectral phase filtering 1)*: As a result of TPM₁, the FSR-divided comb acquires a spectral phase $\phi_{k;p_1,q_1}$ (Figure 7(a.1)), where p_1 is given by Equation (7) (with $s \leftarrow p_1$, $p \leftarrow s_1$ and
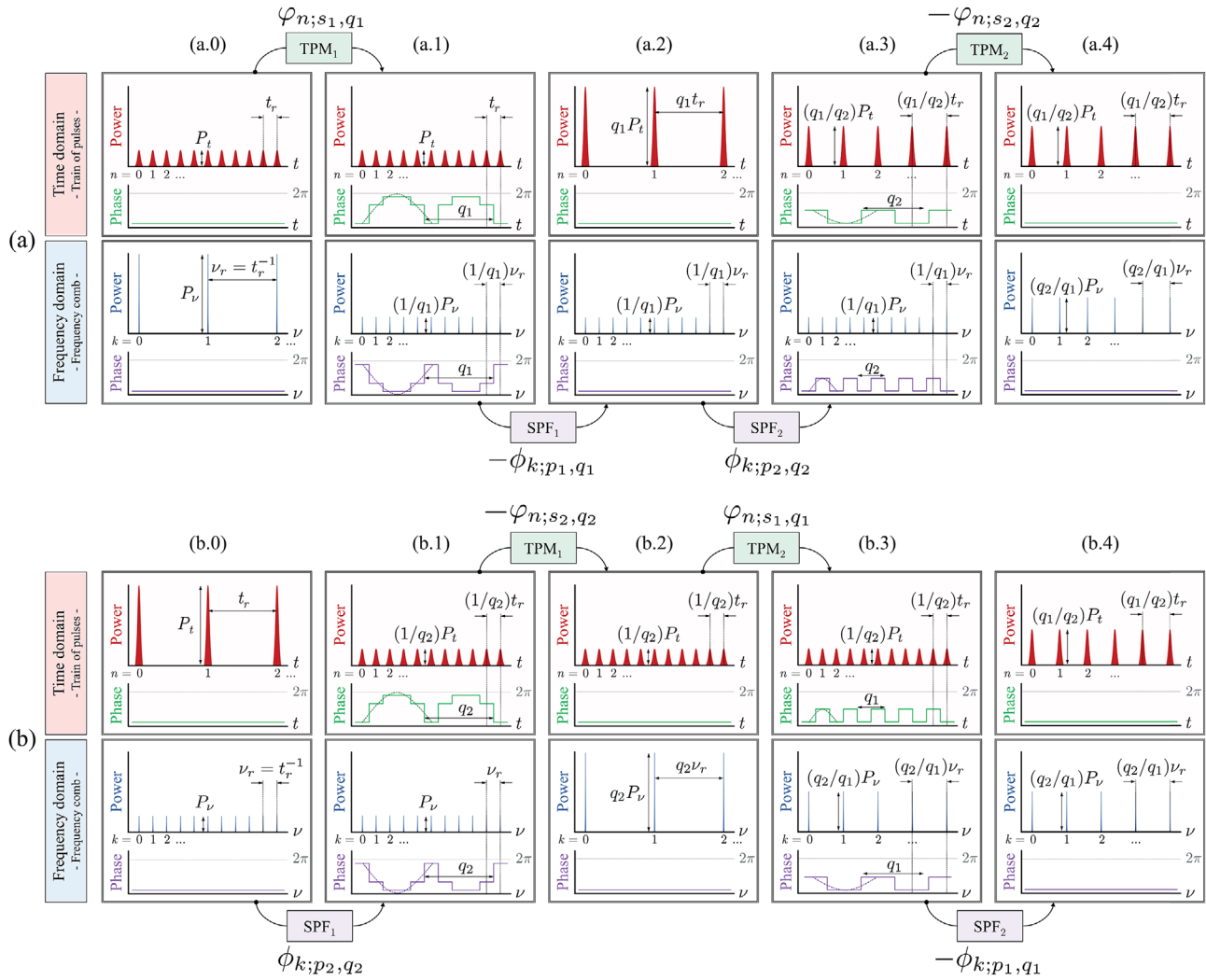
Figure 7. Methods to control the repetition period based on the time/frequency duality of the Talbot effect. a) Phase-controlled temporal Talbot method, and b) phase-controlled spectral Talbot method (see text). TPM: temporal phase modulation; SPF: spectral phase filtering. In both cases, an input pulse train with period t_r (and corresponding input frequency comb with FSR ν_r) is redistributed into an output train with period $q_2^{-1}q_1 t_r \forall \{q_1 q_2\} \epsilon \mathbb{N}$ (and corresponding input frequency comb with FSR $q_1^{-1} q_2 \nu_r$).

$q \leftarrow q_1$). This phase is cancelled by an all-pass frequency filter with the exact opposite phase profile, $-\phi_{k;p_1,q_1}$, resulting in a train of pulses with repetition period $q_1 t_r$ (Figure 7(a.2)). Note that this process can be implemented as linear dispersive propagation, and the required amount of GVD, $\beta_2 z$, can be calculated by substituting $p \leftarrow p_1$, $q \leftarrow q_1$ and $t_r \leftarrow q_1 t_r$ in Equation (3). At this point, the initial train of pulses, with period t_r, has been transformed into another train of pulses with period $q_1 t_r$ with no pulse-to-pulse phase variations. If the desired temporal period multiplication factor is integer, this is the final step.

3. *SPF₂ (spectral phase filtering 2)*: The application of a second spectral phase $\phi_{k;p_2,q_2}$ (corresponding to a temporal Talbot condition p_2/q_2) divides the temporal repetition period of the train obtained after SPF₁ by q_2. If q_1 and q_2 are mutually prime natural numbers, the overall effect is the multiplication of the input pulse period by the fraction $r = q_2^{-1}q_1$ (Figure 7(a.3)).

Note that, depending on the designed values of q_1 and q_2, this factor can be either higher or lower than 1.

4. *TPM₂ (temporal phase modulation 2)*: Finally, since the train of pulses obtained after SPF₂ (Figure 7(a.3)) is a Talbot sub-image of the train obtained after SPF₁ (Figure (7a.2)), there will be uncompensated pulse-to-pulse temporal phase variations. These phases can be cancelled out by the application of an additional TPM step with the sequence $-\varphi_{n;s_2,q_2}$, where s_2 is given by Equation (8) (with $s \leftarrow s_2$, $p \leftarrow p_2$ and $q \leftarrow q_2$). The inverse of the temporal period multiplication factor will then affect the FSR of the obtained output comb, becoming $r^{-1}\nu_r$ (Figure 7(a.4)).

The problem can be reduced to the calculation of four Talbot conditions. Since there are, in general, several allowed values of p (or s) for each value of q (or m),[69] many configurations of the method are possible to achieve a desired value of r. In particular,

**ADVANCED
SCIENCE NEWS**

www.advancedsciencenews.com

**LASER
& PHOTONICS
REVIEWS**

www.lpr-journal.org

Table 1. Phase-controlled temporal Talbot method, general solution.

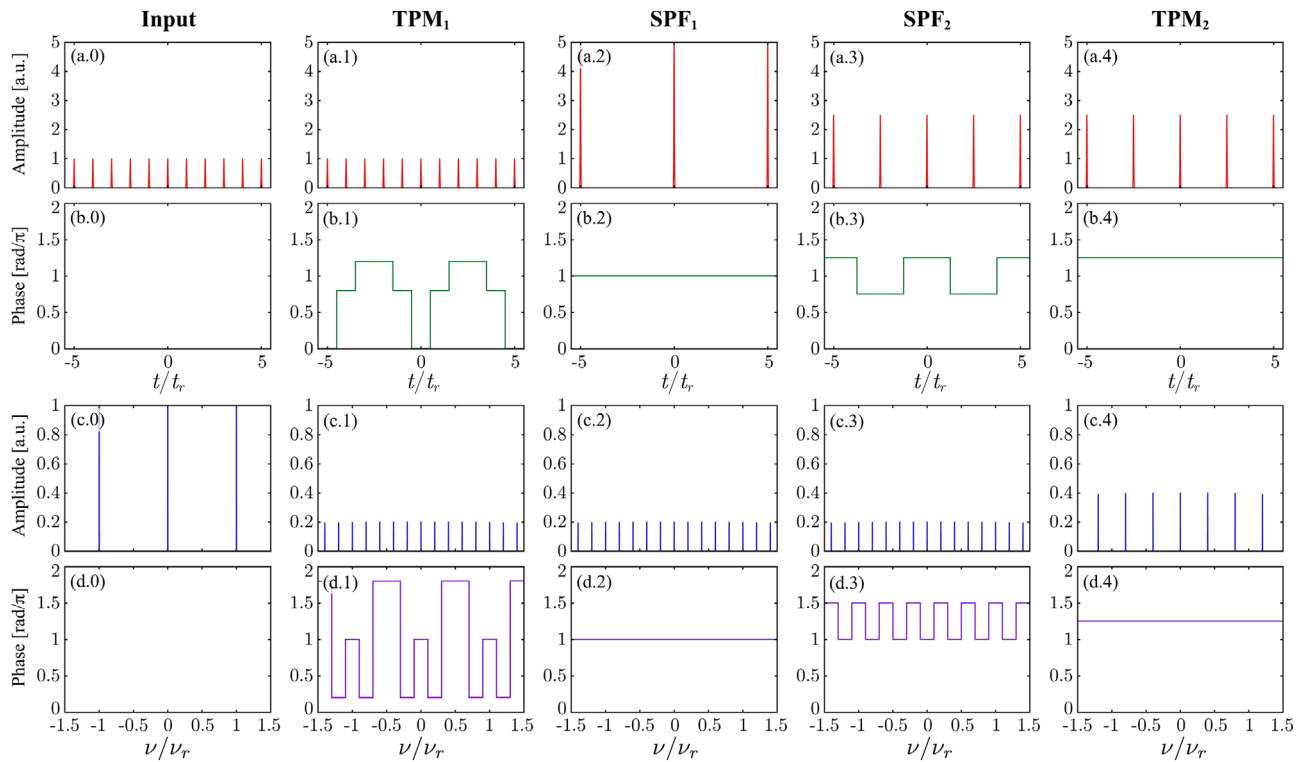| Step	0. Input	1. TPM$_1$	2. SPF$_1$	3. SPF$_2$	4. TPM$_2$
Applied Talbot phase		$\varphi_{n;s_1,q_1}$	$-\phi_{k;p_1,q_1}$	$\phi_{k;p_2,q_2}$	$-\varphi_{n;s_2,q_2}$
		s_1 free	$p_1 \leftarrow$ Equation (8) $\{s_1, q_1\}$	p_2 free	$s_2 \leftarrow$ Equation (8) $\{p_2, q_2\}$
Pulse repetition period	t_r	t_r	$q_1 t_r$	$q_2^{-1} q_1 t_r$	$q_2^{-1} q_1 t_r$
Time domain					
Free spectral range	ν_r	$q_1^{-1}\nu_r$	$q_1^{-1}\nu_r$	$q_1^{-1}\nu_r$	$q_1^{-1}q_2\nu_r$
Frequency domain					

Figure 8. Numerical simulation of the phase-controlled temporal Talbot method (following the steps depicted in Figure 7a) with $r = 5/2$. a) Normalized instantaneous power, b) temporal phase, c) normalized power spectral density, and d) spectral phase. The phase profiles shown have been sampled at the center of each pulse/line in order to facilitate the interpretation of the figure.

s_1 and p_2 are free parameters. **Table 1** summarizes the general solution of the phase-controlled temporal Talbot method, and **Figure 8** shows a step-by-step numerical simulation example, illustrating the results of the application of the phase-controlled temporal Talbot method to multiply the repetition period of a pulse train by the factor $r = 5/2 = 2.5$ (and the FSR of its corresponding frequency comb representation by $r^{-1} = 2/5 = 0.4$). In this simulation, Gaussian pulses with a full width at half maximum equal to 30^{-1} times the pulse repetition period (normalized to 1) are used for ease of interpretation. This produces a frequency comb that remains mostly flat within the chosen spectral representation window. **Figure 9** shows the involved transformations on the temporal Talbot carpet for the particular simulated example ($r = 5/2$).

The methodology outlined here allows for arbitrary control of the repetition period of a pulse train, where the FSR of its frequency comb representation is related to the achieved pulse
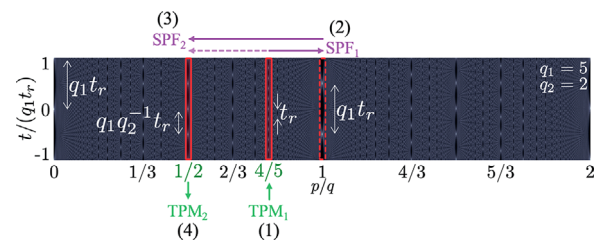

Figure 9. Transformations on the temporal Talbot carpet performed by the phase-controlled temporal Talbot method. The shown example corresponds to $r = 5/2$.

period (the obtained FSR is the exact inverse of the obtained pulse period). Pulse period control techniques proposed to date based on this methodology only deal with temporal period control; consequently, they end with step 3 (Figure 7(a.3)) for fractional pulse period multiplication/division, or step 2 (Figure 7(a.2)) for

**ADVANCED
SCIENCE NEWS**

www.advancedsciencenews.com

**LASER
& PHOTONICS
REVIEWS**

www.lpr-journal.org

integer pulse period multiplication (see Section 5).[63–65] Step 4 (TPM$_2$, Figure 7(a.4)) is only necessary if one wishes to obtain an output pulse train free of pulse-to-pulse phase variations and/or to control the comb FSR accordingly.

As a note on implementation, the two consecutive spectral phase filtering steps, SPF$_1$ and SPF$_2$, can be combined into a single one, imposing a total spectral phase $\phi_{k;p_2,q_2} - \phi_{k;p_1,q_1}$

$$
\begin{aligned}
\phi_{k;p_2,q_2} - \phi_{k;p_1,q_1} &= \sigma_2 \frac{p_2}{q_2} k^2 - \sigma_1 \frac{p_1}{q_1} k^2 \\
&= \frac{\sigma_2 q_1 p_2 - \sigma_1 q_2 p_1}{q_1 q_2} k^2
\end{aligned}
\tag{10}
$$

If this process is implemented as GVD propagation, the total amount of dispersion can always be designed to be smaller than the sum of the magnitudes of both dispersive propagation steps taken independently. This is due to the fact that σ_2, the sign of $\phi_{k;p_2,q_2}$, can be chosen arbitrarily, and σ_1, the sign of $\phi_{k;p_1,q_1}$, is determined by the sign of $\varphi_{n;s_1,q_1}$, which can be set arbitrarily as well.

All the applied transformations are phase-only manipulations. This means that, except for typical insertion losses associated to specific components in a practical system implementation, the total energy of the original pulse train is fundamentally preserved, obtaining an output pulse train where each individual pulse has r times the energy of each individual input pulse. Such transformations only affect the coherent part of the processed signal, and do not have an impact on its incoherent noise content. As a result, the noise content of the input signal, relative to the energy content of its individual pulses, is reduced when $r > 1$.[63] Furthermore, since each individual output pulse is generated from the interference of many consecutive input pulses, aperiodicity in the input signal resulting in variations between input pulses (e.g., pulse-to-pulse intensity and timing fluctuations) are averaged out in the output train.[82] These interesting properties are reviewed in more detail in Section 5.

4.1.2. Particular Solution for Minimum Required Dispersion

As mentioned above, the only restrictions in setting the parameters s_1 and p_2 are that s_1 and q_1 must be mutually prime and have opposite parity, and that p_2 and q_2 must be mutually prime (see Equation (6) and the related explanations). This implies that several solutions to the method can be found for a desired period multiplication factor, $r = q_2^{-1} q_1$.

In particular, it is interesting to look for solutions that minimize the total displacement on the temporal Talbot carpet, since such solutions achieve a minimal required amount of dispersion. From an implementation perspective, this is an attractive design specification, as it minimizes the total propagation length and, in turn, the associated propagation loss.

As per Equation (3) and Table 1, the magnitude of the total required dispersion to achieve the desired period multiplication factor is

$$
2\pi |\beta_2| z = \left| \frac{p_2}{q_2} - \frac{p_1}{q_1} \right| (q_1 t_r)^2
\tag{11}
$$

Recall that the value of p_1 is determined by the values of q_1 and s_1.

From Equation (11), it can be demonstrated that for any q_1 and q_2 coprime, there exist values of p_1 and p_2 that minimize the total dispersion magnitude, and that this minimum value is

$$
2\pi |\beta_2| z = \frac{q_1}{q_2} t_r^2
\tag{12}
$$

For details on the mathematical derivation leading to this result, as well as the guidelines to calculate the parameters s_1 and p_2, see Appendix A.

It is interesting to note that, since q_1 and q_2 are mutually prime naturals, the minimum dispersion defined by Equation (12) satisfies a fractional temporal Talbot condition for the input period t_r (see Equation (3)). In particular, in the absence of the first temporal phase modulation step, TPM$_1$, the method will produce a train of pulses with period $q_2^{-1} t_r$.

4.2. Phase-Controlled Spectral Talbot Method

Here, we define a generalized version of the spectral Talbot effect, that is, a method to transform an optical frequency comb with FSR ν_r into a new comb with FSR $r^{-1} \nu_r$, where the multiplication factor of the FSR, r^{-1}, is any irreducible fraction, that is, $r \in \mathbb{Q}$. Similarly to the temporal version of the method, if the transformation is entirely completed, in the time domain, this translates into a multiplication of the corresponding pulse repetition period by the factor r, that is, from $t_r = \nu_r^{-1}$ to $r t_r$. Note that, for a convenient comparison, here we look for the inverse of the period multiplication factor, in order to keep the definition of the parameter r consistent with the one given in the model of the phase-controlled temporal Talbot method; that is, $r = q_2^{-1} q_1 \forall \{q_1, q_2\} \in \mathbb{N}$ and $\{q_1, q_2\}$ is a co-prime pair.

This second version of the method achieves the same result as the previously explained temporal method, but through transformations along the spectral Talbot carpet (Figure 7b). Once again, the problem is reduced to calculating four Talbot conditions, and just as in the phase-controlled temporal Talbot method, a number of specifications can be adjusted freely in the calculation of the Talbot phases to achieve a desired value of r, leading to many different possible values for the main design parameters.

In the following, we describe the general solution of the problem and then provide guidelines to achieve particular solutions that minimize the displacement on the temporal Talbot carpet.

4.2.1. General Solution with Perfect Phase Cancellation

The phase transformations involved in the general phase-controlled spectral Talbot method can be regarded as the Fourier-dual phase manipulations of the transformations involved in the general phase-controlled temporal Talbot method. The following four steps summarize the method:

0. *Input*: The starting point of the method is a frequency comb with FSR ν_r, corresponding to a train of optical pulses with period $t_r = \nu_r^{-1}$ (Figure 7(b.0)).

**ADVANCED
SCIENCE NEWS**

www.advancedsciencenews.com

LASER
& PHOTONICS
REVIEWS

www.lpr-journal.org

Table 2. Phase-controlled spectral Talbot method, general solution.

Step	0. Input	1. SPF$_1$	2. TPM$_1$	3. TPM$_2$	4. SPF$_2$
Applied Talbot phase		$\phi_{k;p_2,q_2}$	$-\varphi_{n;s_2,q_2}$	$\varphi_{n;s_1,q_1}$	$-\phi_{k;p_1,q_1}$
		p_2 free	$s_2 \leftarrow$ Equation (8) $\{p_2, q_2\}$	s_1 free	$p_1 \leftarrow$ Equation (8) $\{s_1, q_1\}$
Pulse repetition period	t_r	$q_2^{-1} t_r$	$q_2^{-1} t_r$	$q_2^{-1} t_r$	$q_2^{-1} q_1 t_r$
Time domain					
Free spectral range	ν_r	ν_r	$q_2 \nu_r$	$q_1^{-1} q_2 \nu_r$	$q_1^{-1} q_2 \nu_r$
Frequency domain					

1. *SPF$_1$ (spectral phase filtering 1)*: The input comb is phase-filtered with the sequence $\phi_{k;p_2,q_2}$. The resulting pulse train has a period $q_2^{-1} t_r$, while the comb FSR remains equal to ν_r (Figure 7(b.1)).

2. *TPM$_1$ (temporal phase modulation 1)*: The acquired temporal phase is cancelled by a phase modulation mechanism with the opposite phase profile, $-\varphi_{n;s_2,q_2}$. The result is a flat-phase comb with FSR $q_2 \nu_r$ (Figure 7(b.2)). If the desired FSR multiplication factor is integer, this is the final step. The parameter s_2 is given by Equation (7) (with $s \leftarrow s_2$, $p \leftarrow p_2$ and $q \leftarrow q_2$).

3. *TPM$_2$ (temporal phase modulation 2)*: A second temporal phase $\varphi_{k;s_1,q_1}$ divides the FSR by q_1. If q_2 and q_1 are mutually prime natural numbers, the overall effect is the division of the input FSR by the rational factor $r = q_2^{-1} q_1$, resulting in $r^{-1} \nu_r$ (Figure 7(b.3)). Again, this factor can be higher or lower than 1.

4. *SPF$_2$ (spectral phase filtering 2)*: The residual spectral phases, acquired due to the application of TPM$_2$, can be cancelled out by the application of an additional all-pass filtering step, corresponding to $-\phi_{k;p_1,q_1}$, where p_1 is given by Equation (7) (with $s \leftarrow p_1$, $p \leftarrow s_1$ and $q \leftarrow q_1$). The obtained pulse period will then be equal to rt_r.

Similarly to the temporal case, the methodology outlined here allows for arbitrary control of the FSR of a frequency comb, where the pulse period of its temporal train representation is related to the achieved FSR (the obtained pulse period is the exact inverse of the obtained FSR). FSR control techniques proposed to date based on this methodology only deal with spectral period control; consequently, they end with step 3 (Figure 7(b.3)) for fractional FSR multiplication/division, or step 2 (Figure 7(b.2)) for integer FSR multiplication (see Section 5).[67] Step 4 (TPM$_2$, Figure 7(b.4)) is only necessary if one wishes to obtain an output frequency comb free of line-to-line phase variations and/or to control the temporal pulse period accordingly.

Table 2 summarizes the general solution of the phase-controlled spectral Talbot method, and **Figure 10** shows the involved transformations on the spectral Talbot carpet for a particular example with $r^{-1} = 5/2$.

As a note on implementation, the two consecutive phase modulation steps, TPM$_1$ and TPM$_2$, can be combined into a single one, imposing a total temporal phase $\varphi_{n;s_1,q_1} - \varphi_{n;s_2,q_2}$.

$$\varphi_{n;s_1,q_1} - \varphi_{n;s_2,q_2} = -\sigma_1 \frac{s_1}{q_1} n^2 + \sigma_2 \frac{s_2}{q_2} n^2$$

$$= -\frac{\sigma_1 q_2 s_1 - \sigma_2 q_1 s_2}{q_2 q_1} k^2 \quad (13)$$
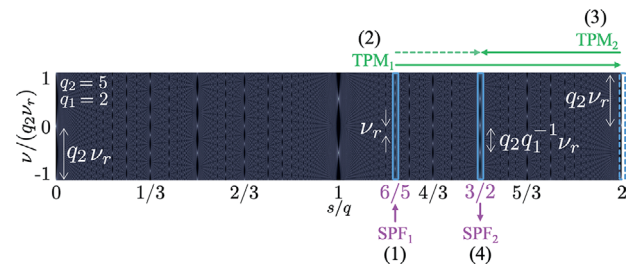

Figure 10. Transformations on the spectral Talbot carpet performed by the phase-controlled spectral Talbot method. The shown example corresponds to $r^{-1} = 5/2$.

where σ_1, the sign of $\varphi_{n;s_1,q_1}$, can be chosen arbitrarily, and σ_2, the sign of $\varphi_{n;s_2,q_2}$, is determined by the sign of $\phi_{k;p_2,q_2}$, which can be set arbitrarily as well.

Conservation of energy ensures that the output comb lines have r^{-1} times the energy of the individual input lines. This energy redistribution only affects the coherent components of the input signal that satisfy the designed Talbot conditions, leading to an effect of noiseless spectral amplification of the individual output comb lines when $r < 1$.[67]

4.2.2. Particular Solution for Minimum Required Dispersion

Since the two spectral phase filtering steps, SPF$_1$ and SPF$_2$, are not consecutive in the phase-controlled spectral Talbot method, the total required dispersion is obtained by adding the magnitudes of both dispersion steps (i.e., without sign).

$$2\pi |\beta_2| z = \frac{p_2}{q_2} t_r^2 + \frac{p_1}{q_1} \left(\frac{q_1}{q_2} t_r \right)^2 \quad (14)$$

In this situation, the minimum displacement in the temporal Talbot carpet is achieved by minimizing each individual displacement induced by SPF$_1$ and SPF$_2$, that is, by imposing $p_2 = 1$ (s_2 is then obtained from Equation (8)), and setting s_1 to obtain $p_1 = 1$ using Equation (8). The minimum dispersion writes then

$$2\pi |\beta_2| z = \frac{q_1 + q_2}{q_2^2} t_r^2 \quad (15)$$

1900176 (11 of 24)

ADVANCED
SCIENCE NEWS

www.advancedsciencenews.com

LASER
& PHOTONICS
REVIEWS

www.lpr-journal.org

4.3. Practical Considerations of Talbot-Based Methods

4.3.1. Limits of the Multiplication Factor

There is a lower limit to the designed period multiplication factor, imposed by the ratio of the pulsewidth to the initial pulse period. In short, the output pulse period must be long enough to accommodate the duration of consecutive output pulses. Considering that in Talbot-based period control methods, the output pulses preserve the temporal shape of the input ones, if Δt is the full-width pulse duration, the pulse period multiplication factor $r = q_2^{-1} q_1$ must satisfy the following condition:

$$\frac{q_1}{q_2} \geq \frac{\Delta t}{t_r} \tag{16}$$

This condition can be equivalently enunciated in the frequency domain, where the limit now deals with the number of discrete frequency components that fit within the pulse bandwidth. The FSR multiplication factor $r^{-1} = q_1^{-1} q_2$ must be such that the output FSR fits within the signal bandwidth, corresponding to the bandwidth of a single input pulse. If $\Delta \nu$ is the full pulse bandwidth, the condition writes

$$\frac{q_2}{q_1} \leq \frac{\Delta \nu}{\nu_r} \tag{17}$$

It should be noted that, fundamentally, there is neither an upper limit to the pulse period multiplication factor, r, nor a lower one to the FSR multiplication factor, r^{-1}; however, practical limitations in the realization of the SPF and TPM processes may limit the implementation of the method with high values of r or low values of r^{-1}, as these would increase the complexity of the involved Talbot phases (e.g., requiring high values of dispersion and/or the realization of complex temporal modulation patterns), as discussed in Section 4.3.2.

Regarding the accessible range of period multiplication factors, the studied method allows for the design of r factors that can be expressed as an irreducible fraction of two natural numbers, that is, rational factors. Irrational multiplication factors cannot be achieved by the proposed technique. Nonetheless, it is a well-known result of number theory that any real number can be approximated by the ratio of two integers with arbitrary precision. This is known as the Diophantine approximation. Hurwitz's theorem establishes an upper bound to such approximations[94]; for every irrational number, ξ, there are infinite mutually prime integers u and v, such that

$$\left| \xi - \frac{u}{v} \right| < \frac{1}{\sqrt{5} v^2} \tag{18}$$

This result suggests that the proposed method could approximate irrational period multiplication factors with high precision.

4.3.2. Considerations on Practical Implementation

We now study the specifics of the two processes involved in the methods –SPF and TPM– from a practical implementation viewpoint.

Spectral Phase Filtering: Temporal Talbot effect is typically induced by linear propagation through a dielectric medium exhibiting second-order group velocity dispersion. This is due to the fact that the different temporal Talbot conditions are achieved by a quadratic spectral phase of a certain curvature.[58] Optical fibers provide a good approximation to second-order dispersion. While these approximations lose accuracy for pulses with broad bandwidths, as higher order dispersion effects become significant,[95] it is possible to design specific dispersion compensating devices and/or propagation media where these high-order dispersion terms are engineered to provide an overall quadratic spectral phase over the entire pulse bandwidth.[96]

It is important to note that the amount of dispersion, required to induce a temporal Talbot condition, scales with the square of the pulse period (see Equation (3)). This means that lower repetition rate trains will require longer propagation distances in order to produce a given Talbot image, for a fixed value of the second-order dispersion coefficient of the medium, β_2. For example, considering a standard single-mode fiber SMF-28, the nominal value of second-order chromatic dispersion at a central wavelength of 1550 nm is $\approx$17 ps nm^{-1} km^{-1}, with a typical attenuation of 0.275 dB km^{-1}. A repetition rate multiplication factor of 2 for a 10 GHz rate pulse train would then require a fiber propagation length of approximately 36 km, with an associated loss of approximately 10 dB (corresponding to a linear power reduction factor of 10). Propagation loss can be mitigated by the use of special fibers, such as dispersion-compensating fibers, which can be designed to introduce larger amounts of dispersion in shorter propagation lengths. Moreover, linearly chirped fiber Bragg gratings and superimposed linearly chirped fiber Bragg gratings further reduce the required propagation lengths by orders of magnitude.[96,97] These are periodic structures, capable of achieving large amounts of second-order dispersion over broad frequency ranges, and with overall losses that can be below the 1-dB level; for example, a few meters of linearly chirped fiber Bragg grating can compensate the dispersion introduced by hundreds of km of SMF-28 over a frequency bandwidth exceeding several THz, thus substantially reducing the loss associated to the propagation of light in the medium.[82]

In this context, it is also interesting to ask which of the two realizations of the method offers an optimal solution with minimum required dispersion. By comparing the minimum dispersion values in Equations (12) and (15), it is easy to verify that the phase-controlled temporal Talbot method offers a solution with lower dispersion than the phase-controlled spectral Talbot method for integer pulse period or FSR multiplication factors (i.e., for $q_1 = 1$ and/or $q_2 = 1$). However, for strictly fractional multiplication factors (i.e., for $\{q_1, q_2\} > 1$) the phase-controlled spectral Talbot method achieves lower dispersion. For a detailed demonstration of this finding, see Appendix B.

Finally, it is important to note that Talbot phases are inherently discrete, that is, the applied phase must be constant over each period of the initial signal, otherwise distortion will be induced on the signal representation in the dual domain. In fact, temporal Talbot effect can be achieved through a especially designed all-pass filter with a discrete phase profile, introducing a line-by-line spectral Talbot phase sequence.[61] On the other hand, optical fibers and linearly chirped fiber Bragg gratings introduce continuous spectral phase variations. These continuous

**ADVANCED
SCIENCE NEWS**

www.advancedsciencenews.com

LASER
& PHOTONICS
REVIEWS

www.lpr-journal.org

phases represent a good approximation to their discrete counterpart in the case of optical frequency combs, as the linewidth of the comb lines is generally narrow enough to neglect any continuous phase variations occurring within each comb line. In general, the linewidth of a frequency comb increases when aperiodicities are introduced across its temporal pulse train representation.[70] For instance, a sequence of pulses with finite duration will have a comb representation with a relatively broad linewidth. Temporal Talbot effect of such a sequence, implemented through continuous (dispersive) spectral filtering, will result in distortion of the individual output pulses.[98]

Temporal Phase Modulation: The TPM profiles employed in the described methods are sequences of constant phase levels, applied pulse to pulse. This is the form of an ideal temporal Talbot phase, that is, flat within each individual pulse. These phase sequences can be generated electronically and introduced to the train of pulses through electro-optical phase modulation.[63–65] The limiting factor in this implementation is the available electronic bandwidth for arbitrary waveform generation (typically in the range of tens of GHz).

A possible solution to overcome this limit would be to avoid the use of electro-optic components and to implement the Talbot phases optically. In order to do this, one could use a nonlinear effect with properly shaped optical pump pulses to imprint the desired Talbot phase in the train to be processed. Spectral Talbot effect induced by cross-phase modulation (XPM) with parabolic-shaped optical pump pulses has been demonstrated.[66] In this situation, one should consider that conditions must be imposed so that the continuous phase modulation closely approaches the desired discrete Talbot phase distribution. In this regard, the pulses of the input train should be sufficiently narrow so that to avoid the introduction of significant chirp, associated to the temporal phase variations occurring within each pulse. This ultimately leads to undesired distortion of the resulting comb spectral envelope. The specific conditions could be derived as the Fourier-domain counterpart of the equivalent problem studied for temporal Talbot effect.[98] This derivation is outside the scope of the present work.

It is important to note that the temporal Talbot phase associated to the sub-image s/m is m-periodic when reduced modulo 2π (assuming $sm \in \mathbb{E}$). Additionally, since these sequences are derived from quadratic expressions (see Equations (4) and (6)), each period of the sequence is symmetric with respect to its central sample. A single period of the temporal Talbot phase associated to the sub-image s/m can then be constructed with m samples that take values in a set of $\lceil m/2 \rceil$ levels. This is an important consideration for the design of the signal used to imprint such a phase in the temporal modulation process. In the case of electronics-based implementations (e.g., the voltage output of an arbitrary waveform generator), this means that the vertical resolution of the involved digital-to-analog converters must be sufficient to encode $\lceil m/2 \rceil$ voltage levels, and the available depth of memory must be sufficient to store m samples. For TPM realizations based on nonlinear effects, these considerations relate to the period and peak power of the pump signal used to excite the nonlinearity. In this context, Maram et al. numerically studied the tolerance in the precision of the pump power level for spectral Talbot effect based on XPM, concluding that higher FSR division factors require pump signals that resemble more accurately the

ideal profile of the desired temporal Talbot phase,[99] a finding that was later demonstrated experimentally by Lei et al.[66] In the case of electro-optical TPM implementations of spectral Talbot effect, Malacarne et al. numerically studied the robustness against deviations from the ideal Talbot phase patterns, reaching a similar conclusion.[62]

5. Review of Experimental Work on Energy-Preserving Signal Processing of Periodic Waveforms

Several methods for pulse repetition rate and comb FSR control based on the theory outlined in this paper have been proposed in the last few years.[60–68] As described above, these involve a combination of specifically designed TPM and SPF operations; however, they generally end with step 3 of the complete methodology described in Section 4. This section reviews experimental demonstrations of such methodology, as well as applications to problems beyond the control of the repetition period. Interesting features of these experimental demonstrations, such as their impact on the noise content of the involved signals, are commented.

5.1. Energy-Preserving Pulse Period Control by Talbot Effect

Integer temporal Talbot effect was first proposed by Jannson et al., as a method to transmit a periodic temporal signal through long distances, avoiding the associated high levels of chromatic dispersion that would otherwise severely distort the waveform.[57] The phenomenon was later observed experimentally by Andrekson in the propagation of picosecond pulse trains through fiber lengths comparable to those covered by telecommunication submarine cables[100] (first experimental results shown in **Figure 11**). It should be noted that in these demonstrations, the period of the signal of interest was not modified, as integer temporal Talbot effect merely reconstructs the input waveform, preserving its periodicity.

Subsequently, fractional temporal Talbot effect (depicted in Figure 1(a.1)) was demonstrated in optical fibers[101,102]; **Figure 12** shows the results of an experiment by Arahira et al., in which fractional temporal Talbot effect of a mode-locked laser signal was observed by propagation through dispersive fibers. Notice that in these early experiments, no connection was still made with the fractional Talbot self-imaging effect observed in the problem of diffraction of periodic spatial objects. Later on, realizations of temporal Talbot self-imaging using linearly chirped fiber Bragg gratings (LCFBG) for lossless pulse period division –pulse repetition rate multiplication– were proposed,[103] and experimentally demonstrated.[104] **Figure 13** shows a set of pioneering results by Longhi et al.,[104] where a properly designed LCFBG was used to multiply the repetition rate of a mode-locked sequence of pulses by a factor 16 through fractional temporal Talbot effect in a LCFBG.

Fractional temporal Talbot effect has since been widely used as a very simple and efficient way for increasing the repetition rate of mode-locked lasers, even enabling the first demonstrations of stable pulse trains with repetition rates in the THz regime, reported by Meloni et al.,[105] as shown in **Figure 14**.
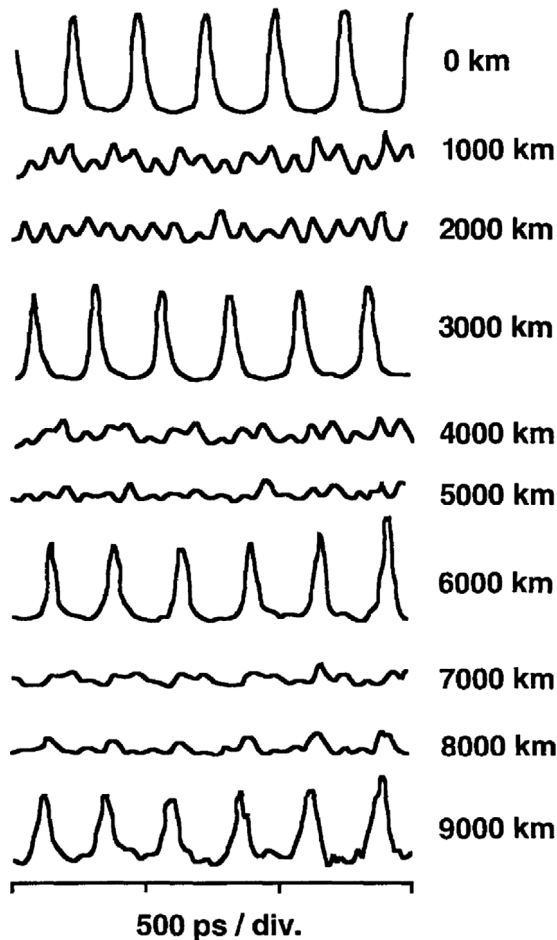
ADVANCED
SCIENCE NEWS

www.advancedsciencenews.com

LASER
& PHOTONICS
REVIEWS

www.lpr-journal.org

Figure 11. Evolution of a 4 GHz periodic pulsed signal in its propagation along 9000 km of optical fiber (traces captured by a streak camera). These results reveal the first experimental observation of integer temporal Talbot images, where the original period and pulse shape are reconstructed, here occurring at multiples of 3000 km. Note how, even in this early demonstration, hints of repetition rate division by 3 – corresponding to fractional temporal Talbot images – are observed at distances of the form $3000p/q$ km with $q = 3$. Reproduced with permission.[100] Copyright 1993, Optical Society of America.

The main advantage of this approach for pulse repetition rate multiplication is its simplicity, as the required SPF transformation can be implemented via a length of optical fiber or a LCFBG. The main drawback of this technique is its limited versatility: Only pulse period division (pulse repetition rate multiplication) by an integer factor is achievable. This is related to the fact that the power spectrum of the processed pulse sequence (including the original FSR) remains unaltered through the process, and as a result, the output rate-multiplied pulse trains acquire deterministic pulse-to-pulse phase variations (mathematical expressions formalized in ref. [69] and explained in Section 3).

The use of phase-controlled Talbot effects, involving an adequate pulse-to-pulse phase conditioning of the pulse train of interest, for example, through an electro-optical TPM process, allowed for a full control of the repetition rate (depicted in Figure 1(b.1)). As described in Section 4, these temporal phase sequences are related to the residual pulse-to-pulse phase variations
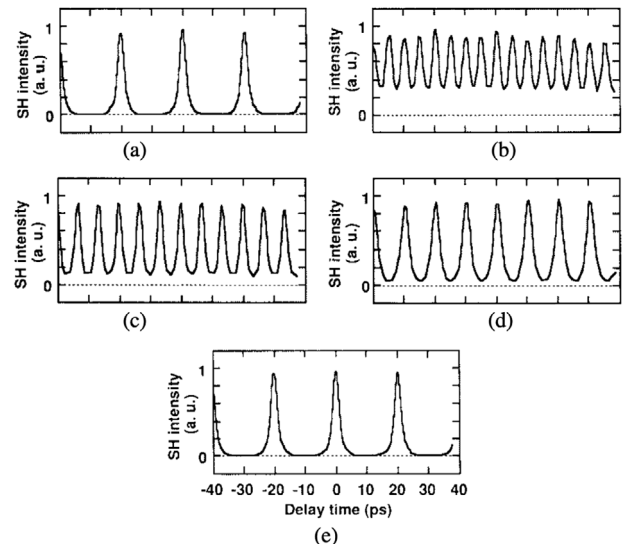

Figure 12. Experimental demonstration of fractional temporal Talbot effect by propagation of a mode-locked pulse train through dispersive fiber. The input repetition rate was approximately 49 GHz, the second-order fiber dispersion was 17.8 ps nm^{-1} km^{-1}, resulting in a Talbot length of 2.87 km. The shown traces correspond to the second-harmonic autocorrelation of the optical signal (10 ps div^{-1}): a) Input pulse train, b) output signal after 720 m of fiber (repetition rate multiplication by 4), c) output signal after 930 m of fiber (repetition rate multiplication by 3), and d) output signal after 1.425 km of fiber (repetition rate multiplication by 2). e) Output signal after 2:87 km of fiber, corresponding to the Talbot length (recovery of the original repetition rate). a–e) Reproduced with permission.[101] Copyright 1998, IEEE.
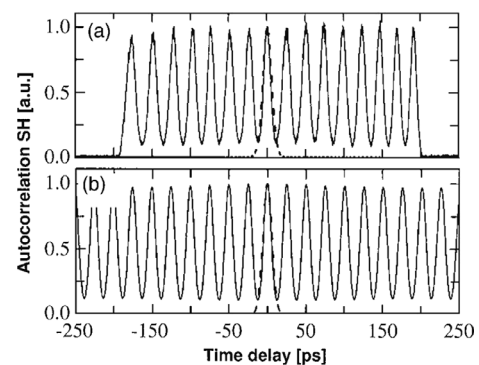

Figure 13. Experimental demonstration of fractional temporal Talbot effect on LCFBGs. a) Numerical and b) experimental autocorrelation traces of a 2.5 GHz pulse train (dashed line) and a 40 GHz pulse train (solid line), obtained by the fractional temporal Talbot effect on an LCFBG, corresponding to a 16-fold multiplication of the input repetition rate. Reproduced with permission.[104] Copyright 2000 Optical Society of America.

acquired by rate-multiplied pulse trains after fractional temporal Talbot effect. Based on this methodology, energy-preserving pulse period multiplication (repetition rate division) of optical pulse trains by integer factors was demonstrated,[63] and later extended to the general case of pulse period multiplication and division by fractional factors.[64,65] The work carried out by Maram et al., illustrated in **Figure 15**, demonstrated energy-preserving pulse repetition period multiplication by temporal Talbot effect with phase-conditioned pulse trains for the first time.
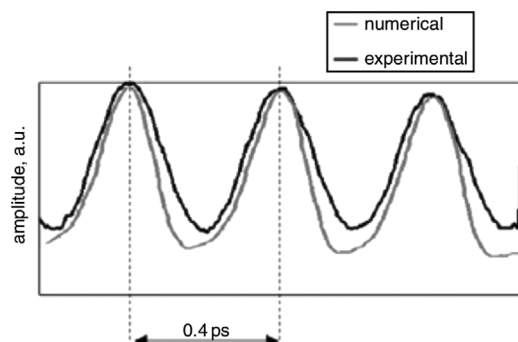
ADVANCED
SCIENCE NEWS
www.advancedsciencenews.com

LASER
& PHOTONICS
REVIEWS

www.lpr-journal.org

Figure 14. Experimental and numerical autocorrelations of a 2.5 THz pulse sequence obtained by 250-fold repetition rate multiplication of a 10 GHz mode-locked laser via the fractional temporal Talbot effect on a single-mode optical fiber. Reproduced with permission.[105] Copyright 2005, IET.

5.1.1. Additional Properties and Extended Functionality

The used phase-only wave transformations in periodicity control of repetitive waveforms, particularly the mentioned operations based on the temporal Talbot effect, imply that the energy of the processed signals is ideally preserved. Furthermore, the wave operations upon which these methods are built (TPM and SPF) can be tailored to produce a user-defined redistribution of the energy content of the signal of interest without affecting the power temporal or spectral densities of any random noise uncorrelated with the signal. This way, if the energy of an input pulse train is redistributed to generate an output pulse train with a longer pulse period, the energy per output pulse will be higher than the energy per input pulse, resulting in an effect of local "passive" amplification of the individual pulses (this effect can be observed in Figure 15). Interestingly, this is achieved without increasing the noise content of the signal. This is in sharp contrast to active gain processes (e.g., as implemented by conventional amplifiers), which not only amplify the noise propagating alongside the signal of interest, but also inject their own external noise contribution, resulting in an unavoidable degradation of the signal-to-noise ratio. Noiseless amplification of periodic intensity waveforms was demonstrated using these techniques in so-called "Talbot amplifiers," including both integer and fractional pulse period multiplication factors. **Figure 16** shows relevant examples of noise mitigation in a Talbot amplifier, reported by Maram et al.[63]

Another interesting characteristic of period control techniques based on energy redistribution is their intrinsic capability to equalize the differences between consecutive pulses. There is no one-to-one relationship between the pulses of an input sequence and the corresponding output pulses obtained by temporal Talbot effect. This is because each output pulse is a product of the interference between many consecutive input pulses, temporally-stretched by dispersive propagation. As a result, differences between input pulses are averaged out in the obtained output train; this is known as the self-healing property of the Talbot effect. These aperiodicities include pulse-to-pulse intensity variations and timing jitter (pulse-to-pulse variations of the repetition rate).

The impact of both integer and fractional temporal Talbot self-healing on the pulse-to-pulse intensity fluctuations of oth-
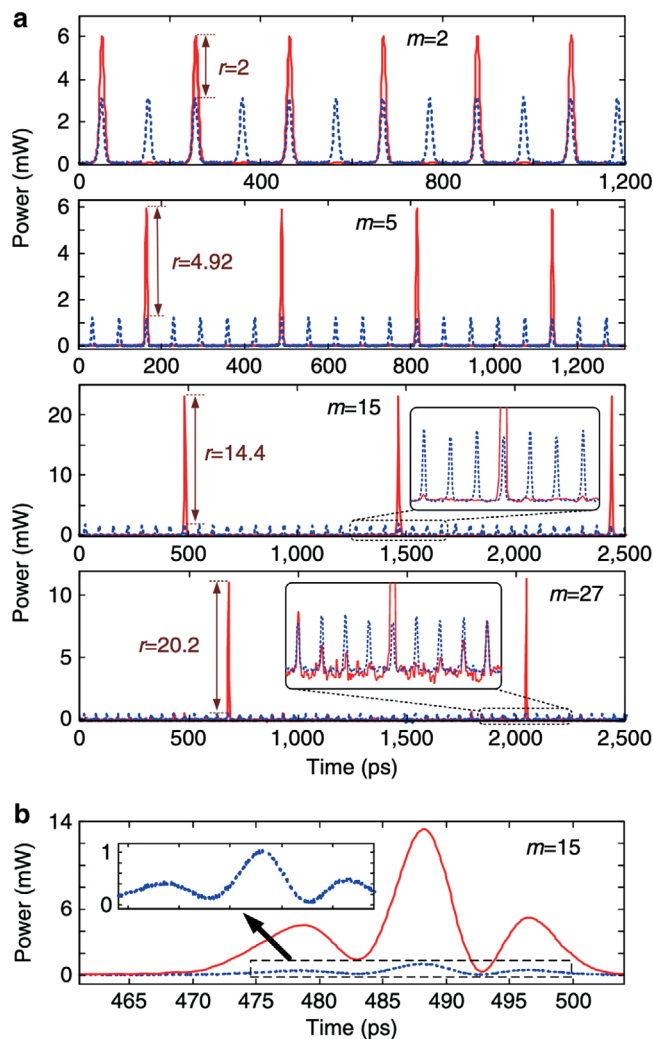

Figure 15. Experimental demonstration of energy-preserving pulse period multiplication by integer factors through the temporal Talbot effect with a phase-conditioned input pulse train. The input pulse trains are shown by the dotted blue lines, while the rate-divided output pulse trains are shown by the solid red lines. The parameter r here refers to the ratio of the output peak power to the input peak power (closely following the designed period division factor, m). a) Pulse period multiplication of a train of Gaussian-like pulses by factors of 2, 5, 15, and 27 (parameter m in the shown plots). b) Detail of the period multiplication process by 15 implemented on a train where the pulses are reshaped, proving that the method is insensitive to the temporal shape of the input pulses. Reproduced under the terms of the CC-BY Creative Commons Attribution 4.0 International License (http://creativecommons.org/licenses/by/4.0/).[63] Copyright 2014, Macmillan Publishers Limited (now Springer Nature).

erwise periodic pulse trains has been the subject of numerous studies.[107–110] In this context, the temporal Talbot effect has been put to practical use for the design of optical clock recovery systems, as demonstrated by Pudo et al. (experimental realization shown in **Figure 17**). Here, the variations in the instantaneous power of a pulsed data-modulated signal, acquired as a result of the introduced data pattern, are equalized, giving rise to a periodic pulse train at a repetition rate matching the clock frequency.[88] This effect is enhanced if Talbot
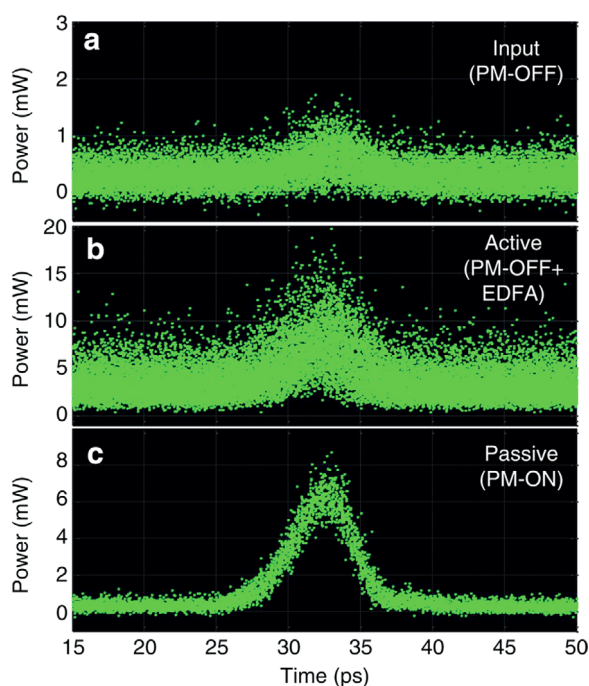
Figure 16. Experimental demonstration of noise mitigation by energy-preserving pulse period multiplication in a Talbot amplifier. a–c) Time traces measured by a sampling oscilloscope without averaging of: a) a noisy pulse with an optical signal-to-noise ratio of 5 (PM-OFF refers to the fact that the TPM process is not operational), b) the pulse amplified by an erbium-doped fiber amplifier (EDFA) with a linear gain factor of 15, and c) the pulse after energy-preserving pulse period multiplication (repetition rate division) by a factor of 15, matching the gain of the amplifier used in (b) (PM-ON refers to the fact that the TPM process is operational). Reproduced under the terms of the CC-BY Creative Commons Attribution 4.0 International License (http://creativecommons.org/licenses/by/4.0/).[63] Copyright 2014, Macmillan Publishers Limited (now Springer Nature).
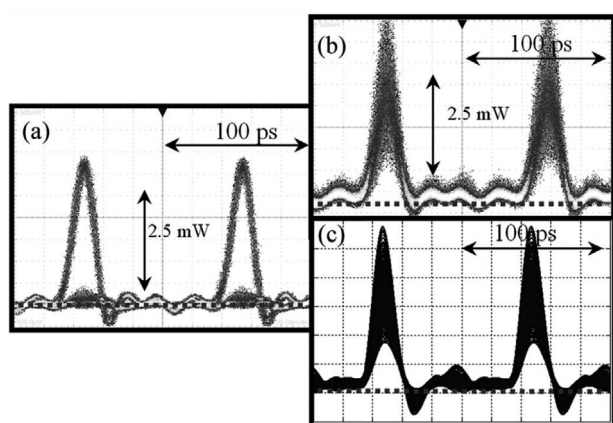

Figure 17. Experimental demonstration of base-rate clock recovery from a sequence of pulses with on–off keying (0/1-binary amplitude) data modulation through the temporal Talbot effect. a) Measured eye diagram of the input data sequence, b) measured eye diagram of the recovered clock signal, and c) numerical simulation of the clock recovery process. Reproduced with permission.[88] Copyright 2017, IEEE.
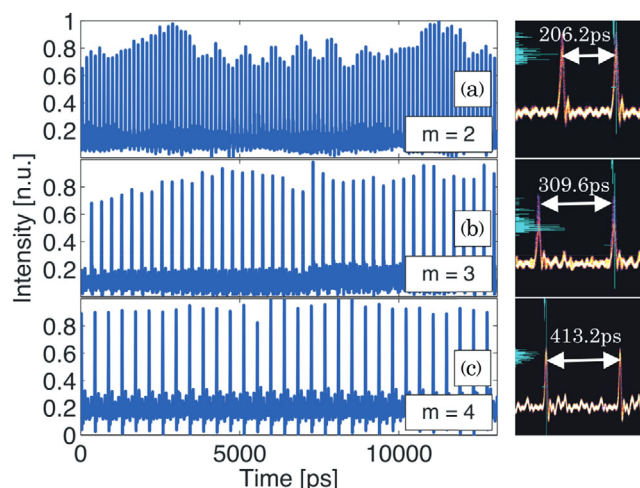

Figure 18. Experimental demonstration of sub-harmonic clock recovery from a sequence of pulses with on–off keying (0/1-binary amplitude) data modulation through temporal Talbot amplification. The recovered clock signal is a decimated version of the base-rate clock by an integer factor (parameter m in the shown plots). a–c) Temporal trace and eye diagrams of recovered clocks at 1/2 (a), 1/3 (b), and 1/4 (c) of the signal's bit rate. It can be seen how the amplitudes of the obtained clock pulses become more equalized as the decimation factor increases. Reproduced with permission.[89] Copyright 2015 Optical Society of America.

amplification is used. In this case, periodic trains at repetition rates corresponding to a decimation of the clock frequency –so-called "sub-harmonic" clock recovery– are generated, featuring output pulses with increased contrast ratios with respect to the pulses obtained in the base-rate case, as demonstrated by Maram et al. (experimental realization show in **Figure 18**).[89]

A similar effect is observed in pulse trains with timing jitter after experiencing temporal Talbot effect. This phenomenon was predicted by Fernández-Pousa et al.,[111–113] with further theoretical analysis by Pudo et al.,[108,114] and experimentally demonstrated by Oiwa et al.[115] Later on, Maram et al. demonstrated that the mitigation of timing jitter is further enhanced in the case of temporal Talbot amplification.[82]

Other interesting applications of pulse repetition rate control via temporal Talbot effect include signal processing systems based on discrete Fourier transforms[116–118] (experimental examples by Xie et al. shown in **Figure 19**), wave-based implementations of prime number factorization algorithms[119] and precise calculation of the dispersion parameters of optical media.[103,120]

It should be noted that all of these operations require the propagation of an optical pulse train through a transparent medium (acting as a spectral phase filter) introducing a specific, fixed amount of second-order group velocity dispersion. It is generally difficult to modify the dispersion parameters of an optical medium once it has been designed, especially for large modifications (e.g., doubling or halving the total amount of introduced dispersion), as these parameters are related to the physical characteristics of the medium. This limits the reconfigurability of these techniques. In order to overcome this limitation, a solution was proposed where a series of dispersive media are interconnected by optical switches, allowing to modify the total dispersion length traversed by the input pulse train of interest.[121] Alternatively, the use of programmable filters,
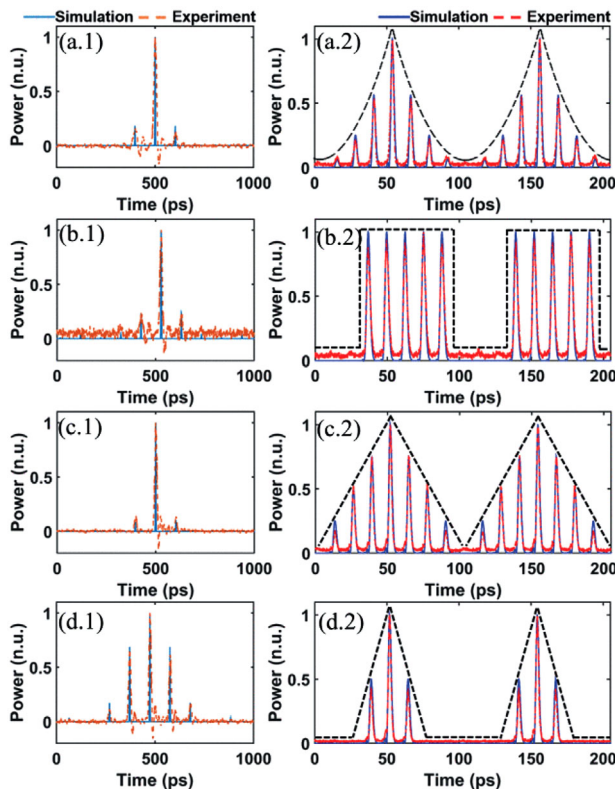
**ADVANCED
SCIENCE NEWS**

www.advancedsciencenews.com

**LASER
& PHOTONICS
REVIEWS**

www.lpr-journal.org

Figure 19. Generation of ultrafast pulse sequences with a user-defined envelope via the temporal Talbot effect of pulse trains with slow-rate amplitude modulation. 1) Modulated input pulses; 2) obtained output pulse sequence with: a) parabolic envelope, b) square envelope, c) triangular envelope, and d) triangular envelope with 50% duty cycle. The envelope of the obtained pulse sequence is determined by the Fourier transform of the applied slow-rate amplitude modulation. Reproduced with permission.[118] Copyright 2018, IEEE.

where the discrete spectrum of the input periodic pulse train is phase-shaped line by line, was used for reconfigurable pulse repetition rate multiplication.[122] In this approach, the programmable filter is configured to introduce the spectral phase profile associated to the desired temporal Talbot sub-image to the input periodic signal, being able to switch between different temporal Talbot conditions by simply reprogramming the filter's transfer function (see experimental results by Caraquitena et al. in **Figure 20**). The main drawbacks of these approaches are their limited reconfiguration speed and the fact that they rely on bulky optical setups. Another solution to the reconfigurability problem, allowing for faster reconfiguration speeds in a more compact setup, consists of modifying the temporal phase profile of the input pulse train prior to dispersive propagation, following a scheme similar to that used in phase-controlled Talbot effects. Indeed, modifying the electrical signal used in conjunction with an electro-optical device to introduce modulation to an optical waveform is a simple task with modern electronic and radio-frequency waveform generation equipment. Advanced designs based on Talbot theory have been proposed for implementation of electronically-programmable pulse repetition rate multiplication techniques, where the dispersive medium responsible for temporal Talbot effect is fixed, and the achieved output repetition rate

can be tuned by modifying the electrical signal driving the phase modulator.[123,124]

Finally, it is worth mentioning that Talbot-based methods have also been used for energy-preserving manipulation of continuous-wave (CW) signals. R. Fernández-Pousa et al. demonstrated efficient CW-to-pulse conversion through a methodology based on the reviewed energy redistribution methods[125] (experimental examples shown in **Figure 21**). This can be interpreted as the time-domain counterpart of the Talbot array illuminator (TAI), a process by which a plane wave is focused into a set of localized bright spots through the interplay of a spatial phase mask and free-space propagation.[91] As such, the process was referred to as a temporal Talbot array illuminator (T-TAI). Additionally, CW-seeded frequency-shifted loop cavities have been demonstrated to produce mode-locked pulse trains by emulating temporal Talbot conditions thanks to the interplay between the cavity roundtrip time and a frequency-shifting element.[68,126,127] Such laser architectures allow for generation of pulse trains from CW sources, with repetition rates tunable in the MHz and GHz regimes.

5.2. Energy-Preserving Comb FSR Control by Talbot Effect

Fractional spectral Talbot effect was proposed,[60,61] and subsequently demonstrated,[62,66] as the Fourier-dual phenomenon of the fractional temporal Talbot effect. As explained in Section 3, this can be utilized for reduction (division) of the FSR of an optical frequency comb by an integer factor through the application of a periodic pulse-to-pulse TPM to the pulse train representation of the comb. The first experimental demonstrations of TPM-induced fractional spectral Talbot effect of a frequency comb were reported by Malacarne et al. (examples shown in **Figure 22**). In these examples, the TPM process is achieved through electro-optical phase modulation driven by a voltage waveform shaped after the necessary Talbot phase pattern. It is also possible to induce this effect to a frequency comb through cross-phase modulation between its pulse train representation and a parabolic-shaped temporal pulse with a suitable level of peak power.[60,66,99] In all these cases, the energy of the original frequency comb is ideally preserved through the process (aside from practical insertion losses) and simply redistributed to build up the output FSR-divided comb.

Similarly to the previously mentioned methods for pulse period control based on the temporal Talbot effect, this approach for FSR manipulation lacks versatility inasmuch as the allowed wave operations are limited to division of the FSR by integer factors. Furthermore, only the power spectrum of the comb is modified by the applied TPM operation, while the instantaneous power of the associated pulse train (including the original pulse period) remains unaffected. As a result, the output FSR-divided frequency combs acquire deterministic line-to-line phase variations (mathematical expressions formalized in ref. [69] and explained in Section 3).

The use of phase-controlled Talbot effects, involving an adequate line-to-line phase conditioning of the frequency comb of interest (e.g., by propagation through a properly-designed second-order group-velocity dispersive medium) allowed for a full control of the FSR (depicted in Figure 1(b.2)). As
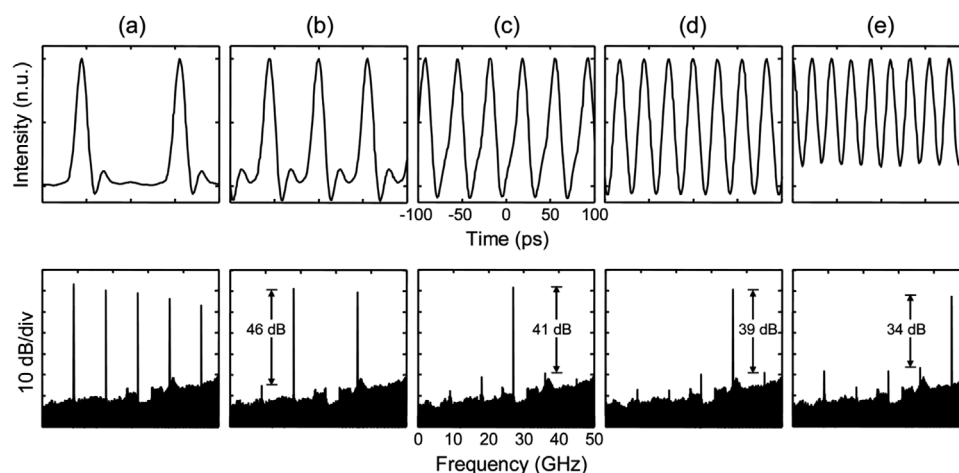
Figure 20. Reconfigurable pulse repetition rate multiplication by temporal Talbot effect in a programmable line-by-line pulse shaper spectral filter. a–e) Oscilloscope traces (top) and associated radio-frequency spectra (bottom) of: a) the input pulse train of interest and b–e) rate-multiplied pulse trains by factors 2, 3, 4, and 5, respectively (obtained by modifying the spectral phase profile introduced by the programmable filter). Reproduced with permission.[122] Copyright 2007, Optical Society of America.
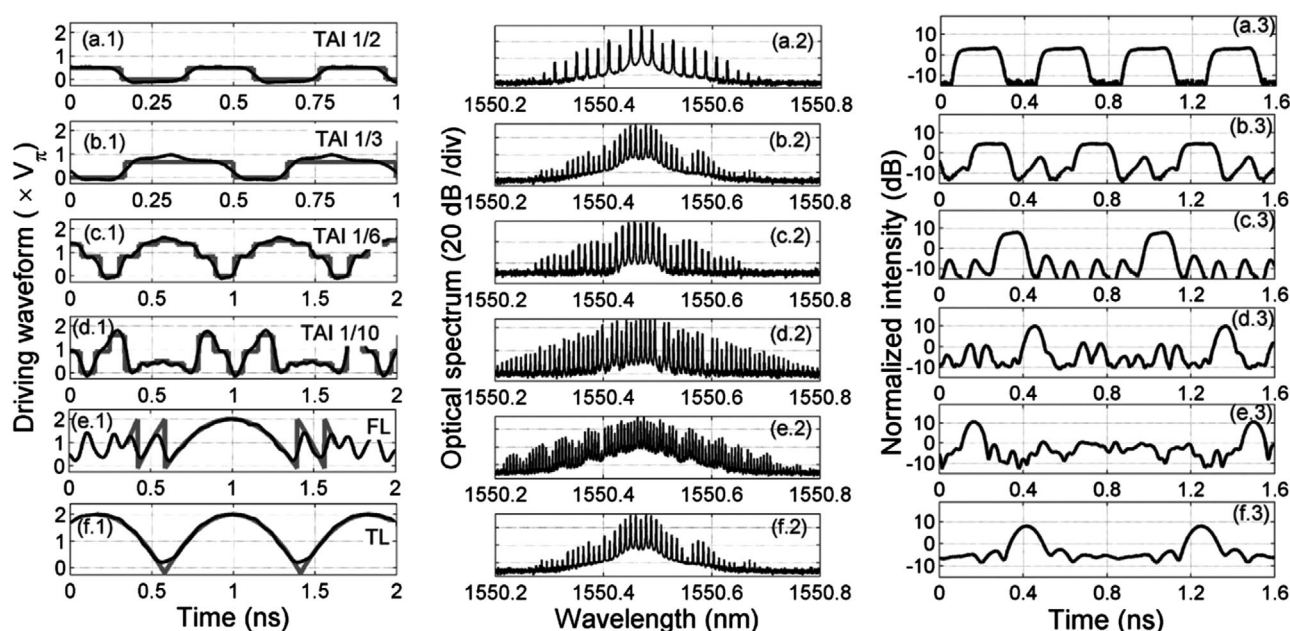

Figure 21. a–f) Generation of pulse sequences from CW light by temporal energy redistribution using temporal Talbot phases to achieve duty cycles of 1/2, 1/3, 1/6, and 1/10 (a–d), the temporal counterpart of a Fresnel lens (e), and a parabolic time lens (f). 1) Temporal phase sequences, 2) optical spectra of the obtained pulse trains, 3) instantaneous power traces of the obtained pulse trains. Reproduced with permission.[125] Copyright 2017, Optical Society of America.

described in Section 4, these spectral phase sequences are related to the residual line-to-line phase variations acquired by FSR-divided combs after fractional spectral Talbot effect. Based on this methodology, energy-preserving arbitrary FSR manipulation was demonstrated by Romero Cortés et al. (experimental examples shown in **Figure 23**).[67] Furthermore, a scheme for user-defined frequency comb generation with FSR reconfigurability over 6 orders of magnitude (from the kHz to the GHz regime) was demonstrated.[68] This was achieved using an acousto-optic frequency shifted feedback laser design for generation of a frequency comb with a reconfigurable quadratic (dispersive) spectral phase profile,[126] combined with Talbot TPM. Other approaches for comb generation and FSR control relying on nonlinear-optics schemes were also demonstrated.[49,50]

5.2.1. Additional Properties and Extended Functionality

As discussed in Section 5.1.1, the use of phase-only transformations translates into the preservation of the energy of the
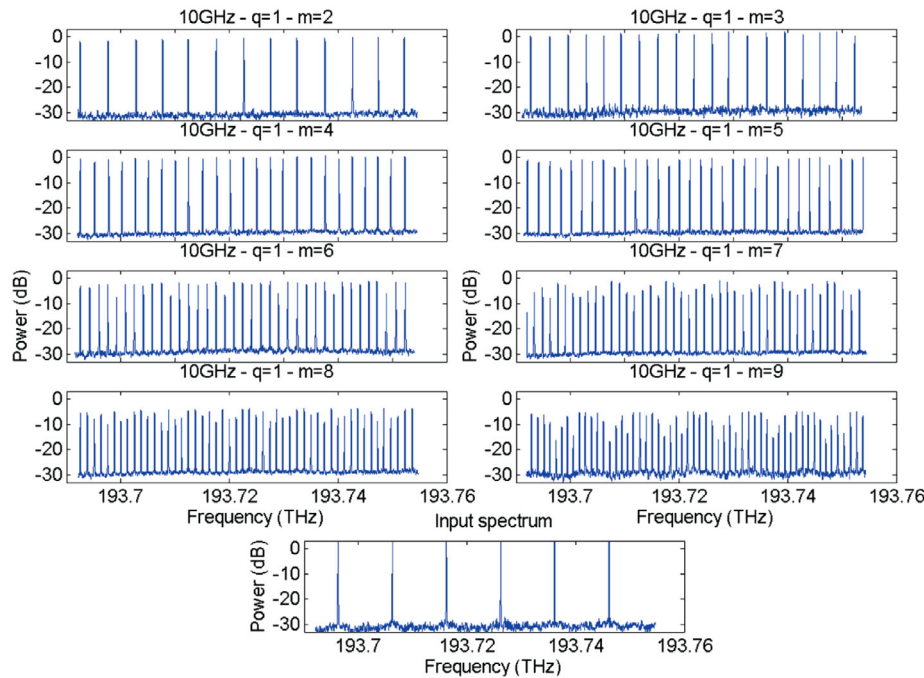
Figure 22. FSR division by integer factors (parameter *m* in the shown plots) through fractional spectral Talbot effect of an optical frequency comb with an FSR of 10 GHz, induced by electro-optical temporal phase modulation. Reproduced with permission.[62] Copyright 2013, Optical Society of America.
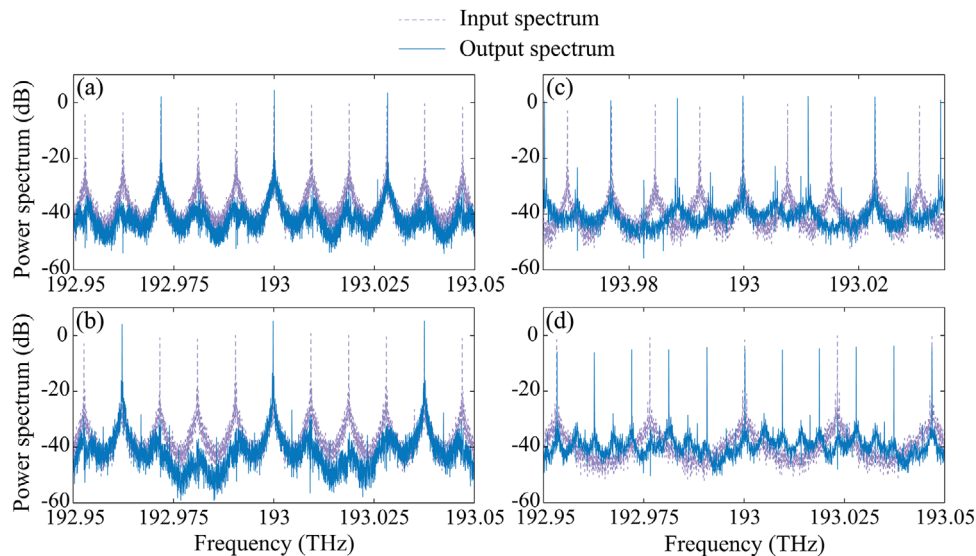

Figure 23. a–d) FSR multiplication by factors r^{-1} = 3 (a), 4 (b), 1.5 (c), and 0.4 (d), induced by combinations of SPF and TPM (original FSR of the input combs: a) 9.463 GHz; b,d) 9.451 GHz; and c) 7.717 GHz).[67] The output frequency combs preserve the envelope and frequency grid of the input ones, and the spectral peak power of the comb lines is modified by the FSR multiplication factor. Adapted with permission.[67] Copyright 2018, American Physical Society.

input comb. In particular, these FSR control methods based on the spectral Talbot effect rely on the same wave operations (SPF and TPM) used by the previously discussed pulse period control methods. As such, they can produce a user-defined redistribution of the energy content of the signal of interest without affecting the power temporal or spectral densities of any random noise uncorrelated with the signal. This way, if the energy of an input frequency comb is redistributed to generate

an output comb with a larger FSR, the energy per output line will be higher than the energy per input line, resulting in an effect of local "passive" amplification of the individual comb lines without increasing the noise content of the signal, in sharp contrast to active gain processes (with their unavoidable signal-to-noise ratio degradation). Romero Cortés et al. demonstrated noiseless spectral amplification of optical frequency combs using these techniques, even achieving extraction of
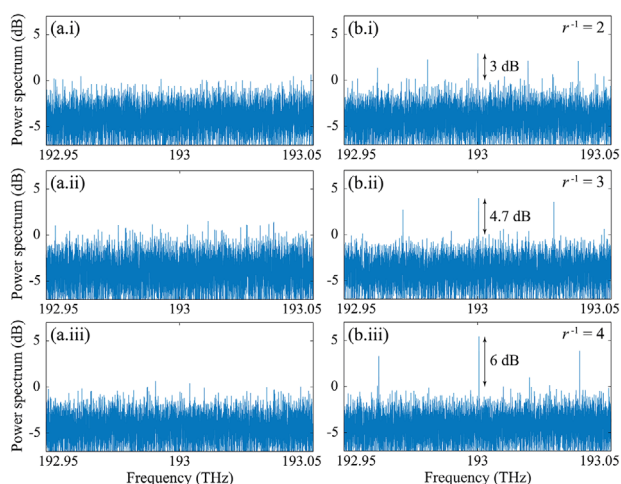
**ADVANCED
SCIENCE NEWS**

www.advancedsciencenews.com

LASER
& PHOTONICS
REVIEWS

www.lpr-journal.org

Figure 24. Sub-noise extraction of frequency combs through noiseless spectral amplification by spectral energy redistribution based on phase-only wave operations.[67] a) Input comb affected by a level of amplified spontaneous emission where the noise level reaches the spectral peak power level of the comb lines. b) Spectral traces of FSR-multiplied combs through energy redistribution (by factors $r^{-1} = 2$ (i), 3 (ii), and 4 (iii)), where the comb lines are raised over the noise floor, increasing their visibility by the FSR multiplication factor (shown here in dB scale). Adapted with permission.[67] Copyright 2018, American Physical Society.

frequency combs from underneath the spectral noise floor when the noise level exceeded that of the comb lines (experimental examples shown in **Figure 24**). It should be noted that this method does not require prior knowledge of the frequencies of the comb lines or the spectral extension of the comb of interest.

It is interesting to note that the mentioned FSR control methods based on the spectral Talbot effect obtain output frequency combs that preserve both the complex spectral envelope and the frequency grid of the input combs. Furthermore, it was recently demonstrated that spectral Talbot effects does not significantly alter the level of phase noise on the reference frequency and FSR of a frequency comb processed through TPM.[128] These are interesting properties for applications that require stabilized frequency combs, such as high-resolution spectroscopy and astronomical measurements through laser-calibrated spectrographs.[3]

Finally, it is worth mentioning that these methods have also been used for energy-preserving manipulation of the continuous broadband spectra of isolated short pulses.[129] This can be interpreted as the frequency-domain counterpart of the temporal TAI, so-called spectral Talbot array illuminator (S-TAI). Romero Cortés et al. used this methodology to reversibly redistribute the spectrum of a short pulse into a periodic sequence of peaks and gaps, leaving broad frequency bands of the pulse's spectrum free of energy (relevant results shown in **Figure 25**). This mechanism has been exploited to demonstrate the first realization of phase-preserving broadband invisibility cloaking.[129]

6. Discussions and Conclusion

In this work, we have presented an in-depth analysis of the fundamental theory behind signal processing methods for periodic-
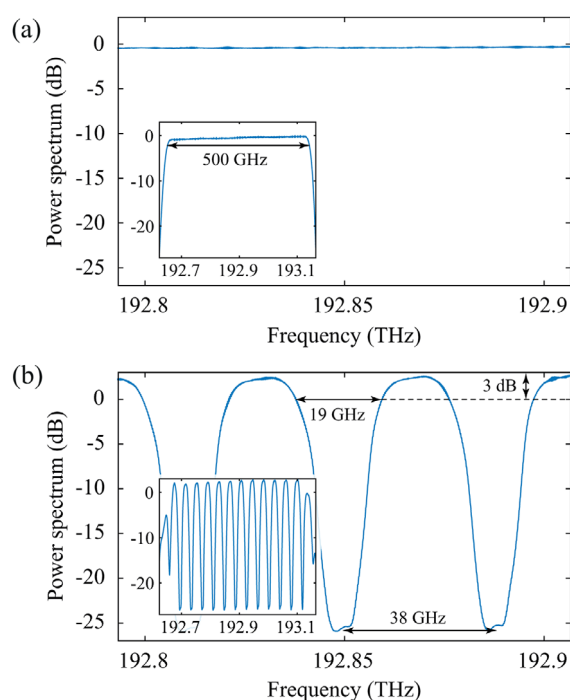

Figure 25. Redistribution of a 500 GHz-wide continuous spectrum into a periodic series of peaks and gaps through wave transformations identical to those used in the phase-controlled spectral Talbot method.[129] a) Input spectrum. b) Output spectrum. Reproduced with permission.[129] Copyright 2018, Optical Society of America.

ity control of repetitive temporal and spectral waveforms based on Talbot effects. These methods inherently preserve the overall energy of the processed wave and perform the desired period manipulation without affecting the features (duration and shape) of the individual temporal pulses and spectral envelope of the pulse train/frequency comb. In particular, we have derived the complete set of energy-preserving transformations necessary to achieve a prescribed, user-defined control of the temporal and spectral periods of repetitive waveforms in both domains simultaneously. Previous works on Talbot-based waveform manipulation have been reviewed and contextualized.

The methods described in this work are particularly interesting for applications that require the ability to precisely set the repetition rate of optical pulse trains, such as for generation and processing of telecommunication signals, arbitrary optical and radio-frequency waveforms, etc. Additionally, disciplines that rely on manipulations of the FSR of frequency combs with high energy efficiency could also benefit from the methods reported here. For instance, energy-preserving FSR multiplication could produce frequency combs with large frequency spacings (well into the GHz regime) and improved side-lobe suppression, a feat of critical importance for comb-based astronomical measurements.[76] Similarly, energy-preserving FSR division could readily enhance the spectral resolution of methods for frequency comb-based spectroscopy. A key advantage of the Talbot methods is that they offer the additional capability to mitigate critical amplitude and phase noise present in the original pulse trains and frequency combs. Moreover, all the operations required by the Talbot methods are linear manipulations of the phase of a wave, along its two

**ADVANCED
SCIENCE NEWS**

www.advancedsciencenews.com

LASER
& PHOTONICS
REVIEWS

www.lpr-journal.org

Fourier-dual domains of representation, for example, time and frequency. This suggests the possibility to extend these methods to any system or framework described by wave equations. In particular, these methods could be readily-applied to the space and transverse momentum –angular spectrum– domains of optical fields, by direct application of the space-time duality.[83] A similar realization of the generalized Talbot method was reported to control the periodicity of repetitive images in two dimensions, even allowing to tailor the spatial repetition periods associated to each dimension independently.[130]

More generally, the operations involved in the reported methods would allow to implement arbitrary period control of signals outside the realm of optical waves. In fact, manifestations of the Talbot effect have been reported across a wide variety of wave regimes, such as radio-frequency waves,[131] acoustic and mechanical waves,[132] X-ray diffraction,[133] matter waves,[134] and quantum wavefunctions,[135] among others. Furthermore, given the beneficial noise-reduction properties of the studied processes,[63,65,67] purely computational versions of these methods could be envisioned to enhance signals and images affected by noise through numerical signal processing operations.

Last but not least, as mentioned above, beyond their interest for application to the control of repetitive waveforms, the outlined wave energy redistribution strategies could be generalized to a wider variety of signal processing scenarios, such as for manipulation of arbitrary aperiodic signals.[125,129] Hence, the Talbot-based methodology outlined and reviewed herein opens a myriad of promising new avenues for advanced arbitrary energy-efficient waveform generation, processing and control, of potential broad practical interest.

Appendix A: Minimum Dispersion in the Phase-Controlled Temporal Talbot Method

Equation (11) gives the dispersion magnitude required in the phase-controlled temporal Talbot method. Renaming $d := 2\pi|\beta_2|z$

$$d = \left|\frac{p_2}{q_2} - \frac{p_1}{q_1}\right| q_1^2 t_r^2 \tag{A1}$$

Equation (A1) rewrites as

$$|p_2 q_1 - p_1 q_2| = \frac{q_2}{q_1}\frac{d}{t_r^2} \tag{A2}$$

Bézout identity states that given two nonzero integers, q_1 and q_2, with greatest common divisor c, there exist integers p_2 and p_1 such that[136]

$$p_2 q_1 - p_1 q_2 = c \tag{A3}$$

where c is the smallest natural number that can be written as $p_2 q_1 - p_1 q_2$ (note that the Bézout coefficients, p_2 and p_1, are not unique, and every integer of the form $p_2 q_1 - p_1 q_2$ is a natural multiple of c). Since q_1 and q_2 are mutually prime, their greatest common divisor is $c = 1$. Using Equation (A3) in Equation (A2), we have the minimum value of d

$$d_{\min} = \frac{q_1}{q_2} t_r^2 \tag{A4}$$

The minimum required dispersion is then fixed by the period multiplication factor, $r = q_2^{-1} q_1$, and the input temporal period, t_r. The associated Bézout coefficients, p_2 and p_1, that satisfy Equation (A3) are determined by the standard extended Euclidean algorithm.[136] Given the specifications for the input period and the desired multiplication factor, r, the parameters of the phase-controlled temporal Talbot method with minimum dispersion can be obtained as follows:

0. Specifications of the method: $r = q_2^{-1} q_1$, and t_r. The minimum dispersion is given by Equation (A4).
1. Determine p_1 and p_2 from Equation (A3) with $c = 1$, using the standard extended Euclidean algorithm.[136]
2. Determine s_1 from p_1 and q_1, using Equation (8).
3. Determine s_2 from p_2 and q_2, using Equation (8).

Appendix B: Comparison of Dispersion Requirements

Equations (12) and (15) give the minimum dispersion values required by the phase-controlled temporal and spectral Talbot methods, respectively. Dropping the constant multiplicative factor t_r^2 on the right-hand side of Equations (12) and (15), and renaming the remaining fractions d_T and d_S, respectively, we have

$$d_T = \frac{q_1}{q_2} \tag{B1a}$$

$$d_S = \frac{q_1 + q_2}{q_2^2} \tag{B1b}$$

We can compare the fractions d_T and d_S by subtracting one from the other or by dividing one by the other.

Proof 1

The difference between d_S and d_T writes

$$d_S - d_T = \frac{q_1 + q_2 - q_1 q_2}{q_2^2} \tag{B2}$$

Since q_2 is real and nonzero, the sign of this fraction is determined by its numerator. In particular, if $q_1 = 1$ and/or $q_2 = 1$, then $q_1 + q_2 > q_1 q_2$, and $d_S > d_T$. On the other hand, if $\{q_1, q_2\} > 1$, then $q_1 + q_2 < q_1 q_2$, and $d_S < d_T$.

Proof 2

The ratio of d_S to d_T writes

$$\frac{d_S}{d_T} = \frac{1}{q_1} + \frac{1}{q_2} \tag{B3}$$

**ADVANCED
SCIENCE NEWS**

www.advancedsciencenews.com

LASER
& PHOTONICS
REVIEWS

www.lpr-journal.org

Since q_1 and q_2 are positive and nonzero, if $q_1 = 1$ and/or $q_2 = 1$, then $q_1^{-1} + q_2^{-1} > 1$, and $d_S > d_T$. On the other hand, if $\{q_1, q_2\} > 1$, then $q_1^{-1} + q_2^{-1} < 1$, and $d_S < d_T$.

In conclusion, the phase-controlled temporal Talbot method offers a solution with lower dispersion than the phase-controlled spectral Talbot method when either the pulse-period or FSR multiplication factor is an integer (i.e., for $q_1 = 1$ and/or $q_2 = 1$). However, for strictly fractional multiplication factors (i.e., for $\{q_1, q_2\} > 1$) the phase-controlled spectral Talbot method achieves lower dispersion.

Conflict of Interest

The authors declare no conflict of interest.

[1] P. W. Smith, *Proc. IEEE* **1970**, *58*, 1342.
[2] B. Barviau, C. Finot, J. Fatome, G. Millot, *IEEE Electron. Lett.* **2007**, *43*, 886.
[3] S. A. Diddams, *J. Opt. Soc. Am. B* **2010**, *27*, B51.
[4] X. Xue, Y. Xuan, P. Wang, Y. Liu, D. E. Leaird, M. Qi, A. M. Weiner, *Laser Photonics Rev.* **2015**, *9*, L23.
[5] V. Brasch, M. Geiselmann, T. Herr, G. Lihachev, M. H. P. Pfeiffer, M. L. Gorodetsky, T. J. Kippenberg, *Science* **2016**, *351*, 357.
[6] X. Xue, P. Wang, Y. Xuan, M. Qi, A. M. Weiner, *Laser Photonics Rev.* **2017**, *11*, 1600276.
[7] A. M. Weiner, *Nature Photon.* **2017**, *11*, 533.
[8] S. A. Miller, M. Yu, X. Ji, A. G. Griffith, J. Cardenas, A. L. Gaeta, M. Lipson, *Optica* **2017**, *4*, 707.
[9] A. Pasquazi, M. Peccianti, L. Razzari, D. J. Moss, S. Coen, M. Erkintalo, Y. K. Chembo, T. Hansson, S. Wabnitz, P. Del'Haye, X. Xue, A. M. Weiner, R. Morandotti, *Phys. Rep.* **2018**, *729*, 1.
[10] J. K. Jang, A. Klenner, X. Ji, Y. Okawachi, M. Lipson, A. L. Gaeta, *Nature Photon.* **2018**, *12*, 688.
[11] B. Stern, X. Ji, Y. Okawachi, A. L. Gaeta, M. Lipson, *Nature* **2018**, *562*, 401.
[12] A. L. Gaeta, M. Lipson, T. J. Kippenberg, *Nature Photon.* **2019**, *13*, 158.
[13] H. Bao, A. Cooper, M. Rowley, L. D. Lauro, J. S. T. Gongora, S. T. Chu, B. E. Little, G. L. Oppo, R. Morandotti, D. J. Moss, B. Wetzel, M. Peccianti, A. Pasquazi, *Nature Photon.* **2019**.
[14] M. Zhang, B. Buscaino, C. Wang, A. Shams-Ansari, C. Reimer, R. Zhu, J. M. Kahn, M. Lončar, *Nature* **2019**, *568*, 373.
[15] S. T. Cundiff, A. M. Weiner, *Nat. Photon.* **2010**, *4*, 760.
[16] V. Torres-Company, A. M. Weiner, *Laser Photonics Rev.* **2014**, *8*, 368.
[17] P. Ghelfi, F. Laghezza, F. Scotti, G. Serafino, A. Capria, S. Pinna, D. Onori, C. Porzi, M. Scaffardi, A. Malacarne, V. Vercesi, E. Lazzeri, F. Berizzi, A. Bogoni, *Nature* **2014**, *507*, 341.
[18] J. Wu, X. Xu, T. G. Nguyen, S. T. Chu, B. E. Little, R. Morandotti, A. Mitchell, D. J. Moss, *IEEE J. Sel. Top. Quantum Electron.* **2018**, *24*, 6101020.
[19] D. Marpaung, J. Yao, J. Capmany, *Nature Photon.* **2019**, *13*, 80.
[20] F. Wang, H. Nong, T. Fobbe, V. Pistore, S. Houver, S. Markmann, N. Jukam, M. Amanti, C. Sirtori, S. Moumdji, R. Colombelli, L.Li, E. Linfield, G. Davies, J. Mangeney, J. Tignon, S. Dhillon, *Laser Photonics Rev.* **2017**, *11*, 1700013.
[21] S. A. Diddams, L. Hollberg, V. Mbele, *Nature* **2007**, *445*, 627.
[22] I. Coddington, N. Newbury, W. Swann, *Optica* **2016**, *3*, 414.
[23] M. Yu, Y. Okawachi, A. G. Griffith, N. Picqué, M. Lipson, A. L. Gaeta, *Nat. Commun.* **2018**, *9*, 1869.
[24] N. Picqué, T. W. Hänsch, *Nature Photon.* **2019**, *13*, 146.
[25] W. F. McGrew, X. Zhang, H. Leopardi, R. J. Fasano, D. Nicolodi, K. Beloy, J. Yao, J. A. Sherman, S. A. Schäffer, J. Savory, R. C. Brown, S. Römisch, C. W. Oates, T. E. Parker, T. M. Fortier, A. D. Ludlow, *Optica* **2019**, *6*, 448.
[26] C. H. Li, A. J. Benedick, P. Fendel, A. G. Glenday, F. X. Kärtner, D. F. Phillips, D. Sasselov, A. Szentgyorgyi, R. L. Walsworth, *Nature* **2008**, *452*, 610.
[27] T. Steinmetz, T. Wilken, C. Araujo-Hauck, R. Holzwarth, T. W. Hänsch, L. Pasquini, A. Manescau, S. D'Odorico, M. T. Murphy, T. Kentischer, W. Schmidt, T. Udem, *Science* **2008**, *321*, 1335.
[28] P. Roztocki, R. Morandotti, *Nat. Astron.* **2019**, *3*, 135.
[29] A. J. Metcalf, T. Anderson, C. F. Bender, S. Blakeslee, W. Brand, D. R. Carlson, W. D. Cochran, S. A. Diddams, M. Endl, C. Fredrick, S. Halverson, D. D. Hickstein, F. Hearty, J. Jennings, S. Kanodia, K. F. Kaplan, E. Levi, E. Lubar, S. Mahadevan, A. Monson, J. P. Ninan, C. Nitroy, S. Osterman, S. B. Papp, F. Quinlan, L. Ramsey, P. Robertson, A. Roy, C. Schwab, S. Sigurdsson, et al., *Optica* **2019**, *6*, 233.
[30] V. Ataie, E. Temprana, L. Liu, E. Myslivets, B. P. P. Kuo, N. Alic, S. Radic, *J. Lightwave Technol.* **2015**, *33*, 694.
[31] E. Temprana, E. Myslivets, B. P. Kuo, L. Liu, V. Ataie, N. Alic, S. Radic, *Science* **2015**, *348*, 1445.
[32] A. Fülöp, M. Mazur, A. Lorences-Riesgo, Ó. B. Helgason, P. H. Wang, Y. Xuan, D. E. Leaird, M. Qi, P. A. Andrekson, A. M. Weiner, V. Torres-Company, *Nat. Commun.* **2018**, *9*, 1598.
[33] J. Pfeifle, V. Brasch, M. Lauermann, Y. Yu, D. Wegner, T. Herr, K. Hartinger, P. Schindler, J. Li, D. Hillerkuss, R. Schmogrow, C. Weimann, R. Holzwarth, W. Freude, J. Leuthold, T. J. Kippenberg, C. Koos, *Nature Photon.* **2014**, *8*, 375.
[34] P. Marin-Palomo, J. N. Kemal, M. Karpov, A. Kordts, J. Pfeifle, M. H. P. Pfeiffer, P. Trocha, S. Wolf, V. Brasch, M. H. Anderson, R. Rosenberger, K. Vijayan, W. Freude, T. J. Kippenberg, C. Koos, *Nature* **2017**, *546*, 274.
[35] C. Reimer, M. Kues, P. Roztocki, B. Wetzel, F. Grazioso, B. E. Little, S. T. Chu, T. Johnston, Y. Bromberg, L. Caspani, D. J. Moss, R. Morandotti, *Science* **2016**, *351*, 1176.
[36] M. Kues, C. Reimer, P. Roztocki, L. Romero Cortés, S. Sciara, B. Wetzel, Y. Zhang, A. Cino, S. T. Chu, B. E. Little, D. J. Moss, L. Caspani, J. Azaña, R. Morandotti, *Nature* **2017**, *546*, 622.
[37] P. Roztocki, S. Sciara, C. Reimer, L. Romero Cortés, Y. Zhang, B. Wetzel, M. Islam, B. Fischer, A. Cino, S. T. Chu, B. E. Little, D. J. Moss, L. Caspani, J. Azaña, M. Kues, R. Morandotti, *J. Lightwave Technol.* **2018**, *37*, 338.

[38] M. Kues, C. Reimer, J. M. Lukens, W. J. Munro, A. M. Weiner, D. J. Moss, R. Morandotti, *Nature Photon.* **2019**, *13*, 170.

[39] G. P. Agrawal, *Fiber-Optic Communication Systems*, 3rd ed., John Wiley & Sons, New York, **2002**.

[40] R. Paschotta, *Field Guide to Laser Pulse Generation*, SPIE Press, Bellingham, WA **2008**.

[41] D. Kielpinski, O. Gat, *Opt. Express* **2012**, *20*, 2717.

[42] C. G. Jeon, S. Zhang, J. Shin, J. Kim, *Sci. Rep.* **2018**, *8*, 13875.

[43] J. van Howe, C. Xu, *J. Lightwave Technol.* **2006**, *24*, 2649.

[44] J. Azaña, R. Slavik, P. Kockaert, L. Chen, S. LaRochelle, *J. Lightwave Technol.* **2003**, *21*, 1490.

[45] J. Magné, J. Bolger, M. Rochette, S. LaRochelle, L. R. Chen, B. J. Eggleton, , J. Azaña, *J. Lightwave Technol.* **2006**, *25*, 2091.

[46] N. B. Hébert, V. Michaud-Belleau, S. Magnan-Saucier, J. D. Deschênes, J. Genest, *Opt. Lett.* **2016**, *41*, 2282.

[47] R. Maram, L. Romero Cortés, J. van Howe, J. Azaña, *J. Lightwave Technol.* **2017**, *35*, 658.

[48] X. Z. Li, J. Azaña, *IEEE J. Sel. Top. Quantum Electron.* **2018**, *25*, 1100310.

[49] Q. Xie, B. Zheng, C. Shu, *IEEE Photon. Technol. Lett.* **2018**, *30*, 975.

[50] B. Zheng, Q. Xie, C. Shu, *J. Lightwave Technol.* **2018**, *36*, 2651.

[51] H. F. Talbot, *Philos. Mag.* **1836**, *9*, 401.

[52] L. Rayleigh, *Philos. Mag.* **1881**, *11*, 196.

[53] K. Patorski, *Prog. Optics* **1989**, *27*, 1.

[54] M. V. Berry, S. Klein, *J. Mod. Opt.* **1996**, *43*, 2139.

[55] S. Matsutani, Y. Ônishi, *Found. Phys. Lett.* **2003**, *16*, 325.

[56] J. Wen, Y. Zhang, M. Xiao, *Adv. Opt. Photon.* **2013**, *5*, 83.

[57] T. Jannson, J. Jannson, *J. Opt. Soc. Am.* **1981**, *71*, 1373.

[58] J. Azaña, M. A. Muriel, *IEEE J. Sel. Top. Quant. Electron.* **2001**, *7*, 728.

[59] G. P. Agrawal, *Nonlinear Fiber Optics*, 4th ed., Academic Press, San Diego, CA **2006**.

[60] J. Azaña, *Opt. Lett.* **2005**, *30*, 227.

[61] J. Caraquitena, M. Beltrán, R. Llorente, J. Martí, M. A. Muriel, *Opt. Lett.* **2011**, *36*, 858.

[62] A. Malacarne, J. Azaña, *Opt. Express* **2013**, *21*, 4139.

[63] R. Maram, J. V. Howe, M. Li, J. Azaña, *Nat. Commun.* **2014**, *5*, 5163.

[64] R. Maram, J. V. Howe, M. Li, J. Azaña, *Opt. Lett.* **2015**, *40*, 375.

[65] L. Romero Cortés, R. Maram, J. Azaña, *Phys. Rev. A* **2015**, *92*, 041804(R).

[66] L. Lei, J. Huh, L. Romero Cortés, R. Maram, B. Wetzel, D. Duchesne, R. Morandotti, J. Azaña, *Opt. Lett.* **2015**, *40*, 5403.

[67] L. Romero Cortés, R. Maram, H. Guillet de Chatellus, J. Azaña, *Phys. Rev. Applied* **2018**, *9*, 064017.

[68] H. Guillet de Chatellus, L. Romero Cortés, J. Azaña, *Opt. Express* **2018**, *26*, 21069.

[69] L. Romero Cortés, H. Guillet de Chatellus, J. Azaña, *Opt. Lett.* **2016**, *41*, 340.

[70] A. V. Oppenheim, A. S. Willsky, S. H. Nawab, *Signals and Systems*, 2nd ed., Prentice-Hall, Upper Saddle River, NJ **1996**.

[71] J. Kim, Y. Song, *Adv. Opt. Photonics* **2016**, *8*, 465.

[72] P. Petropoulos, M. Ibsen, M. N. Zervas, D. J. Richardson, *Opt. Lett.* **2000**, *25*, 521.

[73] X. Xie, R. Bouchand, D. Nicolodi, M. Giunta, W. Hänsel, M. Lezius, A. Joshi, S. Datta, C. Alexandre, M. Lours, P. A. Tremblin, G. Santarelli, R. Holzwarth, Y. L. Coq, *Nat. Photon* **2017**, *11*, 44.

[74] C. Grivas, R. Ismaeel, C. Corbari, C. Huang, D. W. Hewak, P. Lagoudakis, G. Brambilla, *Laser Photonics Rev.* **2018**, *12*, 1800167.

[75] O. de Vries, T. Saule, M. Plötner, F. Lücking, T. Eidam, A. Hoffmann, A. Klenke, S. Hädrich, J. Limpert, S. Holzberger, T. Schreiber, R. Eberhardt, I. Pupeza, A. Tünnermann, *Opt. Express* **2015**, *23*, 19586.

[76] G. Chang, C. H. Li, D. F. Phillips, A. Szentgyorgyi, R. L. Walsworth, F. X. Kärtner, *Opt. Express* **2012**, *20*, 24987.

[77] J. E. Toney, *Lithium Niobate Photonics*, Artech House, Norwood, MA **2015**.

[78] C. Li, *Nonlinear Optics: Principles and Applications*, Springer, Singapore **2017**.

[79] E. Udvary, Investigation of semiconductor optical amplifier direct modulation speed, in *2014 16th Int. Conf. on Transparent Optical Networks (ICTON)*, IEEE, Piscataway, NJ **2014**, pp. 1–4.

[80] K. C. Balram, M. I. Davanço, B. R. Ilic, J. H. Kyhm, J. D. Song, K. Srinivasan, *Phys. Rev. Applied* **2017**, *7*, 024008.

[81] Y. Vidne, M. Rosenbluh, T. W. Hänsch, *Opt. Lett.* **2003**, *28*, 2396.

[82] R. Maram, M. Seghilani, J. Jeon, X. Z. Li, L. Romero Cortés, J. van Howe, J. Azaña, *IEEE Photon. Technol. Lett.* **2018**, *30*, 665.

[83] B. H. Kolner, *IEEE J. Quant. Electron.* **1994**, *30*, 1951.

[84] V. Torres-Company, J. Lancis, P. Andrés, *Prog. Optics* **2011**, *56*, 1.

[85] R. Salem, M. A. Foster, , A. L. Gaeta, *Adv. Opt. Photon.* **2013**, *5*, 274.

[86] J. Azaña, H. Guillet de Chatellus, *Phys. Rev. Lett.* **2014**, *112*, 213902.

[87] E. R. Andresen, C. Finot, D. Oron, H. Rigneault, *Phys. Rev. Lett.* **2013**, *110*, 143902.

[88] D. Pudo, M. Depa, L. R. Chen, *J. Lightwave Technol.* **2007**, *25*, 2898.

[89] R. Maram, L. Romero Cortés, J. Azaña, *Opt. Express* **2015**, *23*, 3602.

[90] H. Dammann, G. Groh, M. Kock, *Appl. Opt.* **1971**, *10*, 1454.

[91] A. W. Lohmann, J. A. Thomas, *Appl. Opt.* **1990**, *29*, 4337.

[92] L. Romero Cortés, A. Deville, M. Seghilani, I. Hamam, H. G. de Chatellus, J. Azaña, presented at Imaging and Applied Optics 2017, San Francisco, CA, June **2017**, paper IW4E.2.

[93] C. R. Fernández-Pousa, *J. Opt. Soc. Am. A* **2017**, *34*, 732.

[94] W. M. Schmidt, *Diophantine Approximation*, Springer, Berlin - Heidelberg, Germany **1980**.

[95] J. Fatome, S. Pitois, G. Millot, *Opt. Commun.* **2004**, *234*, 29.

[96] R. Kashyap, *Fiber Bragg Gratings*, 2nd ed., Academic Press, Boston, MA **2010**.

[97] J. Azaña, S. Gupta, *Opt. Express* **2006**, *21*, 4270.

[98] J. Azaña, *J. Opt. Soc. Am. B* **2003**, *20*, 83.

[99] R. Maram, J. Azaña, *Opt. Express* **2013**, *21*, 28824.

[100] P. A. Andrekson, *Opt. Lett.* **1993**, *18*, 1621.

[101] S. Arahira, S. Kutsuzawa, Y. Matsui, D. Kunimatsu, Y. Ogawa, *J. Lightwave Technol.* **1998**, *16*, 405.

[102] I. Shake, H. Takara, S. Kawanishi, M. Saruwatari, *Electron. Lett.* **1998**, *34*, 792.

[103] J. Azaña, M. A. Muriel, *Appl. Opt.* **1999**, *38*, 6700.

[104] S. Longhi, M. Marano, P. Laporta, O. Svelto, M. Belmonte, B. Agogliati, L. Arcangeli, V. Pruneri, M. N. Zervas, M. Ibsen, *Opt. Lett.* **2000**, *25*, 1481.

[105] G. Meloni, G. Berrettini, M. Scaffardi, A. Bogoni, L. Poti, M. Guglielmucci, *Electron. Lett.* **2005**, *41*, 1294.

[106] Creative Commons, Attribution 4.0 International (CC BY 4.0), https://creativecommons.org/licenses/by/4.0/.

[107] D. Pudo, L. R. Chen, *IEEE Photon. Technol. Lett.* **2006**, *18*, 658.

[108] D. Pudo, L. R. Chen, *Opt. Express* **2007**, *15*, 6351.

[109] J. Xing, C. Wang, H. Chi, X. Yu, S. Zheng, X. Jin, X. Zhang, *IEEE Photon. Technol. Lett.* **2018**, *30*, 1376.

[110] H. Chi, J. Xing, S. Yang, T. Jin, *IEEE Access* **2019**, *7*, 86177.

[111] C. R. Fernández-Pousa, F. Mateos, L. Chantada, M. T. Flores-Arias, C. Bao, M. V. Pérez, C. Gómez-Reino, *J. Opt. Soc. Am. B* **2004**, *21*, 1170.

[112] C. R. Fernández-Pousa, F. Mateos, L. Chantada, M. T. Flores-Arias, C. Bao, M. V. Pérez, C. Gómez-Reino, *J. Opt. Soc. Am. B* **2005**, *22*, 753.

[113] L. Chantada, C. R. Fernández-Pousa, M. T. Flores-Arias, C. Gómez-Reino, *Appl. Opt.* **2008**, *47*, E19.

[114] D. Pudo, C. R. Fernández-Pousa, L. R. Chen, *IEEE Photon. Technol. Lett.* **2008**, *20*, 496.

[115] M. Oiwa, J. Kim, K. Tsuji, N. Onodera, M. Saruwatari, in *Conf. on Lasers and Electro-Optics and Conf. on Quantum Electronics and Laser Science*, IEEE, Piscataway, NJ **2008**, pp. 1–2.

[116] V. García-Muñoz, M. A. Preciado, M. A. Muriel, *Opt. Express* **2007**, *15*, 10878.

[117] C. R. Fernández-Pousa, *Opt. Commun.* **2017**, *402*, 97.

[118] Q. Xie, C. Shu, *IEEE Photon. Technol. Lett.* **2018**, *30*, 242.

[119] D. Bigourd, B. Chatel, W. P. Schleich, B. Girard, *Phys. Rev. Lett.* **2008**, *100*, 030202.

[120] C. Cuadrado-Labordea, P. A. Costanzo-Casoa, R. Duchowicza, E. E. Sicre, *Opt. Commun.* **2006**, *260*, 528.

[121] D. Pudo, L. R. Chen, *J. Lightwave Technol.* **2005**, *23*, 1729.

[122] J. Caraquitena, Z. Jiang, D. E. Leaird, A. M. Weiner, *Opt. Lett.* **2007**, *32*, 716.

[123] S. Tainta, M. J. Erro, W. Amaya, M. J. Garde, S. Sales, M. A. Muriel, *IEEE J. Sel. Top. Quantum Electron.* **2012**, *18*, 377.

[124] R. Maram, L. Romero Cortés, J. Azaña, *J. Lightwave Technol.* **2016**, *34*, 448.

[125] C. R. Fernández-Pousa, R. Maram, J. Azaña, *Opt. Lett.* **2017**, *42*, 2427.

[126] H. Guillet de Chatellus, E. Lacot, W. Glastre, O. Jacquin, O. Hugon, *Phys. Rev. A* **2013**, *88*, 033828.

[127] H. G. de Chatellus, O. Jacquin, O. Hugon, W. Glastre, E. Lacot, J. Marklof, *Opt. Express* **2013**, *21*, 15065.

[128] M. Seghilani, X. Z. Li, R. Maram, L. Romero Cortés, J. Azaña, in *2018 Conf. on Lasers and Electro-Optics (CLEO)*, IEEE, Piscataway, NJ **2018**, pp. 1–2.

[129] L. Romero Cortés, M. Seghilani, R. Maram, J. Azaña, *Optica* **2018**, *5*, 779.

[130] H. Guillet de Chatellus, L. Romero Cortés, A. Deville, M. Seghilani, J. Azaña, *Phys. Rev. Lett.* **2017**, *118*, 133903.

[131] M. G. Keller, J. Shaker, Y. M. M. Antar, *IEEE Transactions on Antennas and Propagation* **2008**, *56*, 245.

[132] A. Berezovski, W. X. Tang, W. Wan, *Mech. Res. Commun.* **2014**, *60*, 21.

[133] F. Pfeiffer, T. Weitkamp, O. Bunk, C. David, *Nat. Phys.* **2006**, *2*, 258.

[134] J. Ruostekoski, B. Kneer, W. P. Schleich, G. Rempe, *Phys. Rev. A* **2001**, *63*, 043613.

[135] X. B. Song, H. B. Wang, J. Xiong, K. Wang, X. Zhang, K. H. Luo, L. A. Wu, *Phys. Rev. Lett.* **2011**, *107*, 033902.

[136] V. Shoup, *A Computational Introduction to Number Theory and Algebra*, Cambridge University Press, Cambridge, England **2009**.

1900176 (24 of 24)